

Reliable numerical solution of a class of nonlinear elliptic problems generated by the Poisson-Boltzmann equation

J. Kraus*, S. Nakov†, S. Repin‡

Abstract

We consider a class of nonlinear elliptic problems associated with models in biophysics, which are described by the Poisson-Boltzmann equation (PBE). We prove mathematical correctness of the problem, study a suitable class of approximations, and deduce guaranteed and fully computable bounds of approximation errors. The latter goal is achieved by means of the approach suggested in [25] for convex variational problems. Moreover, we establish the error identity, which defines the error measure natural for the considered class of problems and show that it yields computable majorants and minorants of the global error as well as indicators of local errors that provide efficient adaptation of meshes. Theoretical results are confirmed by a collection of numerical tests that includes problems on 2D and 3D Lipschitz domains.

Keywords: Poisson-Boltzmann equation, semilinear partial differential equations, existence and uniqueness of solutions, convergence of finite element approximations, a priori error estimates, guaranteed and efficient a posteriori error bounds, error indicators, adaptive mesh refinement, qualified and unqualified convergence.

1 Introduction

1.1 Classical statement of the problem

Let $\Omega \subset \mathbb{R}^d$, $d = 2, 3$ be a bounded domain with Lipschitz boundary $\partial\Omega$. Henceforth we assume that Ω contains an interior subdomain Ω_1 with Lipschitz boundary Γ . In general, Ω_1 may consist of several disconnected parts (in this case all of them are assumed to have Lipschitz continuous boundaries). We consider the following class of nonlinear elliptic equations motivated by the Poisson-Boltzmann equation (PBE), which is widely used for computation of electrostatic interactions in a system of biomolecules in ionic solution [17, 8, 9]:

$$-\nabla \cdot (\epsilon \nabla u) + k^2 \sinh(u + w) = l \quad \text{in } \Omega_1 \cup \Omega_2, \quad (1.1a)$$

$$[u]_{\Gamma} = 0, \quad (1.1b)$$

$$\left[\epsilon \frac{\partial u}{\partial n} \right]_{\Gamma} = 0, \quad (1.1c)$$

$$u = 0, \quad \text{on } \partial\Omega, \quad (1.1d)$$

*University of Duisburg-Essen, Germany

†RICAM, Austrian Academy of Sciences

‡University of Jyväskylä, Finland; V. A. Steklov Institute of Mathematics in St. Petersburg, Russia

where $\Omega_2 := \Omega \setminus (\Omega_1 \cup \Gamma)$, the coefficients $\epsilon, k \in L^\infty(\Omega)$, $\epsilon_{\max} \geq \epsilon \geq \epsilon_{\min} > 0$, w is measurable, and $l \in L^2(\Omega)$. Typically, in biophysical applications, Ω_1 is occupied by one or more macromolecules and Ω_2 is occupied by a solution of water and moving ions. The coefficients ϵ and k represent the dielectric constant and the modified Debye-Huckel parameter and u is the dimensionless electrostatic potential. Concerning the given functions k and w , we can identify three main cases:

- (a) $k_{\max} \geq k(x) \geq k_{\min} > 0$ in Ω and $w \in L^\infty(\Omega)$
- (b) $k(x) \equiv 0$ in Ω_1 , $k_{\max} \geq k(x) \geq k_{\min} > 0$ in Ω_2 and $w \in L^\infty(\Omega_2)$
- (c) $k(x) \equiv 0$ in Ω_2 , $k_{\max} \geq k(x) \geq k_{\min} > 0$ in Ω_1 and $w \in L^\infty(\Omega_1)$

Throughout the paper, the major attention is paid to the case (b), which arises when solving the PBE and is the most interesting from the practical point of view. The cases (a) and (c) can be studied analogously (with some rather obvious modifications). The case with nonhomogeneous Dirichlet boundary condition $u = g$ on $\partial\Omega$ can also be treated in this framework provided that the boundary condition is defined as the trace of a function g such that $g \in H^1(\Omega) \cap L^\infty(\Omega)$ and $\nabla g \in L^s(\Omega)$ with $s > \max\{2, d\}$.

The reliable and efficient solution of the nonlinear Poisson Boltzmann equation (PBE) for complex geometries of the interior domain Ω_1 (with Lipschitz boundary) and piecewise constant dielectrics has important applications in biophysics and biochemistry, e.g., in modeling the effects of water and ion screening on the potentials in and around soluble proteins, nucleic acids, membranes, and polar molecules and ions, see [17] and the references therein. Although the solution of the linearized PBE, as in the linear Debye-Huckel theory, often yields accurate approximations [16] certain mathematical models are valid only when based on the nonlinear PBE.

Over the recent years adaptive finite element methods have proved to be an adequate technique in the numerical solution of elliptic problems with local features due to point sources, heterogeneous coefficients or nonsmooth boundaries or interfaces, see e.g., [3, 19] and also successfully used to solve the nonlinear PBE [18, 20]. Adaptivity heavily relies on reliable and efficient error indicators that are typically developed in the framework of a posteriori error control. While the theory of a posteriori error estimates for linear elliptic partial differential equations is already well established and understood, it is far less developed for nonlinear problems. A posteriori error analysis based on functional estimates has already been successfully applied to variational nonlinear problems including obstacle problems in [23, 26]. The accuracy verification approach taken in this work is also based on arguments that are commonly used in duality theory and convex analysis and can be found, e.g. in [15, 21]. Another important issue in the efficient solution of the nonlinear PBE is related to the fast solution of the systems of nonlinear and finally linear algebraic equations that arise from—for instance adaptive finite element—discretization. Multigrid methods may provide optimal or nearly optimal algorithms in terms of computational complexity to perform this task, see, e.g., [13], a topic which is beyond the scope of this paper.

The main questions studied in the paper are related to the well posedness of Problem (1.1) and a posteriori error estimation of its numerical solution. We use a suitable weak formulation (Definition 2.1), where the nonlinearity does not satisfy any polynomial growth condition and consequently it does not induce a bounded mapping from $H_0^1(\Omega)$ to its dual $H^{-1}(\Omega)$. For this (more general) weak formulation we can guarantee the existence of a solution and prove its uniqueness using a result of Brezis and Browder [12]. Additionally, in Proposition 2.1, we show that the solution is bounded (here [12] is used again together

with special test functions suggested in Stampacchia [10, 6]). Boundedness of the solution is important and later used in the derivation of functional a posteriori error estimates. By applying the general framework from [25] and [21] we derive guaranteed and computable bounds of the difference between the exact solution and any function from the respective energy class in terms of the energy and combined energy norms (equations (3.17) and (3.28)). Moreover, we obtain an error equality (3.27) with respect to a certain measure for the error which is the sum of the usual combined energy norm $\|\nabla(v - u)\|^2 + \|y^* - p^*\|_*^2$ and a nonlinear measure. In the case of a linear elliptic equation of the form $-\operatorname{div}(\epsilon \nabla u) + u = l$, this nonlinear measure reduces to $\|v - u\|_{L^2(\Omega)}^2 + \|\operatorname{div}(y^* - p^*)\|_{L^2(\Omega)}^2$, where v and y^* are approximations to the exact solution u and the exact flux $p^* = \epsilon \nabla u$. One advantage of the presented error estimate is that it is valid for any conforming approximations of u and $\epsilon \nabla u$ and that it does not rely on Galerkin orthogonality or properties specific to the used numerical method. Another advantage is that only the mathematical structure of the problem is exploited and therefore no mesh dependent constants are present in the estimate. Majorants of the error not only give guaranteed bounds of global (energy) error norms but also generate efficient error indicators (cf. (1.1a), Figures 13 and 14). Also, we derive a simple, but efficient lower bound for the error in the combined energy norm. Using only the error majorant, we obtain an analog of Cea's lemma which forms a basis for the a priori convergence analysis of finite element approximations for this class of semilinear problems. Finally, we present three numerical examples that verify the accuracy of error majorants and minorants and confirm efficiency of the error indicator in mesh adaptive procedures.

The outline of the paper is as follows. In Section 2, we recall some facts from the duality theory and general a posteriori error estimation method for convex variational problems. Next, we briefly discuss correctness of Problem (1.1) and prove an a priori $L^\infty(\Omega)$ estimate for the solution u . In Section 3, we apply the abstract framework from Section 2 and derive explicit forms of all the respective terms. A special attention is paid to the general error identity that defines a combined error measure natural for the considered class of problems. At the end of Section 3, we prove convergence of the conforming finite element method based on P_1 Lagrange elements. In Section 4, we consider numerical examples in $2D$ and $3D$ and compare the results with solutions obtained by adaptive mesh refinements based on different indicators. The last section includes a summary of the results and comments on possible generalizations of the method to a wider class of nonlinear problems.

2 Abstract framework

First, we briefly recall some results from the duality theory ([21, 15]). Consider a class of variational problems having the following common form:

$$\begin{aligned} &\text{Find } u \in V \text{ such that} \\ (P) \quad &J(u) = \inf_{v \in V} J(v), \text{ where } J(v) = G(\Lambda v) + F(v). \end{aligned} \quad (2.1)$$

Here, V, Y are reflexive Banach spaces with the norms $\|\cdot\|_V$ and $\|\cdot\|_Y$, respectively, $F : V \rightarrow \overline{\mathbb{R}}, G : Y \rightarrow \overline{\mathbb{R}}$ are convex and proper functionals, and $\Lambda : V \rightarrow Y$ is a bounded linear operator. By 0_V we denote the zero element in V . It is assumed that J is coercive and lower semicontinuous. In this case, Problem (P) has a solution u , which is unique if J is strictly convex.

The spaces topologically dual to V and Y are denoted by V^* and Y^* , respectively. They are endowed with the norms $\|\cdot\|_{V^*}$ and $\|\cdot\|_{Y^*}$. Henceforth, $\langle v^*, v \rangle$ denotes the duality

product of $v^* \in V^*$ and $v \in V$. Analogously, (y^*, y) is the duality product of $y^* \in Y^*$ and $y \in Y$. $\Lambda^* : Y^* \rightarrow V^*$ is the operator adjoint to Λ . It is defined by the relation

$$\langle \Lambda^* y^*, v \rangle = (y^*, \Lambda v), \quad \forall v \in V, \forall y^* \in Y^*.$$

We recall that a convex functional $J : V \rightarrow \overline{\mathbb{R}}$ is called *uniformly convex* in a ball $B(0_V, \delta)$ (see, e.g. [21]) if there exists a nonnegative proper and lower semicontinuous functional $\Upsilon_\delta, \Upsilon_\delta : V \rightarrow \overline{\mathbb{R}}$ with $\Upsilon_\delta(v) = 0$ iff $v = 0_V$ such that for all $v_1, v_2 \in B(0_V, \delta)$ the following inequality holds:

$$J\left(\frac{v_1 + v_2}{2}\right) + \Upsilon_\delta(v_1 - v_2) \leq \frac{1}{2}(J(v_1) + J(v_2)). \quad (2.2)$$

The functional Υ_δ enforces the standard midpoint convexity inequality and therefore is called a *forcing* functional.

Remark 2.1. *In what follows, we will use the term forcing functional under slightly weaker conditions than usual hereby dropping the requirement that $\Upsilon(v) = 0$ implies that $v = 0$.*

The functional $J^* : V^* \rightarrow \overline{\mathbb{R}}$ defined by the relation

$$J^*(v^*) := \sup_{v \in V} \{\langle v^*, v \rangle - J(v)\}$$

is called *dual* (or Fenchel conjugate) conjugate to J (see, e.g. [15]). In accordance with the general duality theory of the calculus of variations, the primal Problem (2.1) has a dual counterpart:

$$\begin{aligned} &\text{Find } p^* \in Y^* \text{ such that} \\ (P^*) \quad I^*(p^*) &= \sup_{y^* \in Y^*} I^*(y^*), \text{ where } I^*(y^*) := -G^*(y^*) - F^*(-\Lambda^* y^*), \end{aligned} \quad (2.3)$$

where G^* and F^* are the functionals conjugate to G and F , respectively. The problems (P) and (P^*) are generated by the Lagrangian $L : V \times Y^* \rightarrow \overline{\mathbb{R}}$ defined by the relation

$$L(v, y^*) = (y^*, \Lambda v) - G^*(y^*) + F(v).$$

If we additionally assume that G^* is coercive and that $F(0_V)$ is finite, then it is well known that problems (P) and (P^*) have unique solutions $u \in V$ and $p^* \in Y^*$ and that strong duality relations hold (see [21], or Proposition 2.3, Remark 2.3, and Proposition 1.2 from chapter VI in [15]):

$$J(u) = \inf_{v \in V} J(v) = \inf_{v \in V} \sup_{y^* \in Y^*} L(v, y^*) = \sup_{y^* \in Y^*} \inf_{v \in V} L(v, y^*) = \sup_{y^* \in Y^*} I^*(y^*) = I^*(p^*). \quad (2.4)$$

Furthermore, the pair (u, p^*) is a saddle point for the Lagrangian L , i.e.,

$$L(u, y^*) \leq L(u, p^*) \leq L(v, p^*), \quad \forall v \in V, \forall y^* \in Y^* \quad (2.5)$$

and u and p^* satisfy the relations

$$\Lambda u \in \partial G^*(p^*), \quad p^* \in \partial G(\Lambda u). \quad (2.6)$$

Now let $\Upsilon_G, \Upsilon_{G^*}, \Upsilon_F, \Upsilon_{F^*}$ be forcing functionals for G, G^*, F, F^* , respectively (it is not required that all of them are nontrivial).

Using the linearity of Λ , we find that

$$\begin{aligned}
\Upsilon_G(\Lambda v - \Lambda u) &\leq \frac{1}{2}G(\Lambda v) + \frac{1}{2}G(\Lambda u) - G\left(\frac{\Lambda v + \Lambda u}{2}\right) \\
&\leq \frac{1}{2}G(\Lambda v) + \frac{1}{2}G(\Lambda u) - G\left(\frac{\Lambda v + \Lambda u}{2}\right) + \frac{1}{2}F(v) + \frac{1}{2}F(u) - F\left(\frac{v+u}{2}\right) - \Upsilon_F(v-u) \\
&= \frac{1}{2}J(v) + \frac{1}{2}J(u) - J\left(\frac{v+u}{2}\right) - \Upsilon_F(v-u) \\
&\leq \frac{1}{2}J(v) - \frac{1}{2}J(u) - \Upsilon_F(v-u).
\end{aligned}$$

Similarly,

$$\Upsilon_{G^*}(y^* - p^*) \leq \frac{1}{2}I^*(p^*) - \frac{1}{2}I^*(y^*) - \Upsilon_{F^*}(-\Lambda^*y^* + \Lambda^*p^*).$$

Summing up the above two inequalities and noting that $J(u) = I^*(p^*)$ we obtain the principle error estimate (see [25, 21])

$$\begin{aligned}
&\frac{\Upsilon_G(\Lambda v - \Lambda u) + \Upsilon_{G^*}(y^* - p^*) + \Upsilon_F(v-u) + \Upsilon_{F^*}(-\Lambda^*y^* + \Lambda^*p^*)}{2} \\
&\leq \frac{1}{2}(J(v) - I^*(y^*)) = \frac{1}{2}[G(\Lambda v) + F(v) + G^*(y^*) + F^*(-\Lambda^*y^*)] \\
&= \frac{1}{2}[D_G(\Lambda v, y^*) + D_F(v, -\Lambda^*y^*)] =: \frac{1}{2}M_{\oplus}^2(v, y^*), \tag{2.7}
\end{aligned}$$

where

$$D_G(\Lambda v, y^*) := G(\Lambda v) + G^*(y^*) - \langle y^*, \Lambda v \rangle$$

and

$$D_F(v, -\Lambda^*y^*) := F(v) + F^*(-\Lambda^*y^*) + \langle \Lambda^*y^*, v \rangle$$

are the *compound* functionals for G and F , respectively [21]. A compound functional is nonnegative by the definition. Moreover, the equality

$$J(v) - I^*(y^*) = D_G(\Lambda v, y^*) + D_F(v, -\Lambda^*y^*) = M_{\oplus}^2(v, y^*), \tag{2.8}$$

shows that D_G and D_F can vanish simultaneously if and only if $v = u$ and $y^* = p^*$. The relation (2.7) exposes the general form of the a posteriori error estimate of the functional type expressed in terms of forcing functionals. Moreover, setting $v := u$ and $y^* := p^*$ in (2.8), we obtain analogous identities for the primal and dual parts of the error:

$$J(u) - I^*(y^*) = M_{\oplus}^2(u, y^*) = D_G(\Lambda u, y^*) + D_F(u, -\Lambda^*y^*), \tag{2.9a}$$

$$J(v) - I^*(p^*) = M_{\oplus}^2(v, p^*) = D_G(\Lambda v, p^*) + D_F(v, -\Lambda^*p^*). \tag{2.9b}$$

Using the fact that $J(u) = I^*(p^*)$ and that the above equalities (2.9a), (2.9b) hold, we obtain another important relation (see [21])

$$\begin{aligned}
M_{\oplus}^2(v, y^*) &= J(v) - I^*(y^*) \\
&= J(v) - I^*(p^*) + J(u) - I^*(y^*) = M_{\oplus}^2(v, p^*) + M_{\oplus}^2(u, y^*). \tag{2.10}
\end{aligned}$$

Notice that $M_{\oplus}^2(v, y^*)$ depends on the approximations v and y^* only and, therefore, is fully computable. The right-hand side of (2.10) can be viewed as a certain measure of

the distance between (u, p^*) and (v, y^*) , which vanishes if and only if $v = u$ and $y^* = p^*$. Hence the relation

$$D_G(\Lambda v, p^*) + D_F(v, -\Lambda^* p^*) + D_G(\Lambda u, y^*) + D_F(u, -\Lambda^* y^*) = M_{\oplus}^2(v, y^*) \quad (2.11)$$

establishes the equality of the computable term $M_{\oplus}^2(v, y^*)$ and an error measure natural for this class of variational problems.

It is worth noting that the identity (2.11) can be represented in terms of norms if G and F are quadratic functionals. For example, if $V = H_0^1(\Omega)$, $V^* = H^{-1}(\Omega)$, $Y = [L^2(\Omega)]^d = Y^*$, $G(\Lambda v) = G(\nabla v) = \int_{\Omega} \frac{1}{2} A \nabla v \cdot \nabla v dx$ and $F(v) = \int_{\Omega} (\frac{1}{2} v^2 - lv) dx$ (where A is a symmetric positive definite matrix with bounded entries), then

$$\begin{aligned} D_G(\Lambda v, p^*) &= \frac{1}{2} \int_{\Omega} A \nabla(v - u) \cdot \nabla(v - u) dx, \\ D_F(v, -\Lambda^* p^*) &= \frac{1}{2} \|v - u\|_{L^2(\Omega)}^2, \\ D_G(\Lambda u, y^*) &= \frac{1}{2} \int_{\Omega} A^{-1}(y^* - p^*) \cdot (y^* - p^*) dx, \\ D_F(u, -\Lambda^* y^*) &= \frac{1}{2} \|\operatorname{div}(y^* - p^*)\|_{L^2(\Omega)}^2. \end{aligned} \quad (2.12)$$

In this case, the minimizer of (2.1) solves the linear elliptic problem $-\operatorname{div}(A \nabla u) + u = l$ in Ω and (2.11) is reduced to the error identity

$$\begin{aligned} \int_{\Omega} A \nabla(v - u) \cdot \nabla(v - u) dx + \int_{\Omega} A^{-1}(y^* - p^*) \cdot (y^* - p^*) dx \\ + \|v - u\|_{L^2(\Omega)}^2 + \|\operatorname{div}(y^* - p^*)\|_{L^2(\Omega)}^2 = 2M_{\oplus}(v, y^*)^2. \end{aligned} \quad (2.13)$$

The sum of the first and the third term in (2.13) represents the primal, the sum of the second and fourth term the dual error.

2.1 Variational form of the problem

Definition 2.1. We call u a weak solution of (1.1) if $u \in H_0^1(\Omega)$ and u is such that $b(x, u + w)v \in L^1(\Omega)$ for any $v \in H_0^1(\Omega) \cap L^\infty(\Omega)$ and

$$a(u, v) + \int_{\Omega} b(x, u + w)v dx = \int_{\Omega} l v dx, \quad \forall v \in H_0^1(\Omega) \cap L^\infty(\Omega), \quad (2.14)$$

where $a(u, v) = \int_{\Omega} \epsilon \nabla u \cdot \nabla v dx$ and $b(x, z) := k^2(x) \sinh(z)$.

The problem has the variational form (2.1) if we set $V = H_0^1(\Omega)$ and define $J : H_0^1(\Omega) \rightarrow \mathbb{R} \cup \{+\infty\}$ as follows:

$$J(v) := \begin{cases} \int_{\Omega} \left[\frac{\epsilon(x)}{2} |\nabla v|^2 + k^2 \cosh(v + w) - lv \right] dx, & \text{if } k^2 \cosh(v + w) \in L^1(\Omega_2), \\ +\infty, & \text{if } k^2 \cosh(v + w) \notin L^1(\Omega_2). \end{cases} \quad (2.15)$$

Using the Lebesgue dominated convergence theorem together with the fact that at the minimizer u we have $\cosh(u + w) \in L^1(\Omega)$, it can be seen that the necessary condition for u to be a minimizer of J is

$$\int_{\Omega} \epsilon \nabla u \cdot \nabla v dx + \int_{\Omega} k^2 \sinh(u + w) v dx = \int_{\Omega} l v dx, \forall v \in H_0^1(\Omega) \cap L^\infty(\Omega),$$

which is exactly (2.14). Since $J(v)$ is strictly convex, coercive, and sequentially weakly lower semicontinuous (s.w.l.s) on $H_0^1(\Omega)$ it has a unique minimizer. We note that $J(v)$ is s.w.l.s. because the functional $\int_{\Omega} (\frac{\epsilon}{2} |\nabla v|^2 - lv) dx$ is convex and Gateaux differentiable and, therefore, s.w.l.s. over $H_0^1(\Omega)$ (see Corollary 2.4 in [22]). For $d = 3$, the functional $\int_{\Omega} k^2(x) \cosh(v + w) dx$ is not Gateaux differentiable. In view of Fatou's lemma and the compact embedding of $H_0^1(\Omega)$ into $L^2(\Omega)$ the functional $\int_{\Omega} k^2(x) \cosh(v + w) dx$ is also s.w.l.s.. Uniqueness of the solution of (2.14) follows from the monotonicity property of b , namely,

$$\int_{\Omega} (b(x, v + w) - b(x, z + w)) (v - z) dx \geq 0, \forall v, z \in H_0^1(\Omega).$$

If $u_1, u_2 \in H_0^1(\Omega)$ are two different solutions of (2.14), then

$$a(u_1 - u_2, v) + \int_{\Omega} (b(x, u_1 + w) - b(x, u_2 + w)) v dx = 0, \forall v \in H_0^1(\Omega) \cap L^\infty(\Omega).$$

Now, applying the theorem in [12] to $b(x, u_1 + w) - b(x, u_2 + w) \in H^{-1}(\Omega) \cap L_{loc}^1(\Omega)$ and the function $v = u_1 - u_2 \in H_0^1(\Omega)$, we conclude that

$$a(u_1 - u_2, u_1 - u_2) + \int_{\Omega} (b(x, u_1 + w) - b(x, u_2 + w)) (u_1 - u_2) dx = 0$$

and, consequently, $u_1 = u_2$. We arrive at the following assertion:

Proposition 2.1. *Problem (2.1) has a unique minimizer u , which coincides with the unique weak solution $u \in H_0^1(\Omega)$ of Problem (2.14).*

Next, we show that the solution to Problem (2.14) is essentially bounded. To prove this, we need the following lemma (see [6]).

Lemma 2.1. *Let $\varphi(t)$ denote a function which is nonnegative and nonincreasing for $s_0 \leq t < \infty$. Further, let*

$$\varphi(h) \leq C \frac{\varphi(s)^\beta}{(h - s)^\alpha}, \forall h > s > s_0,$$

where C, α are positive constants and $\beta > 1$. If $e \in \mathbb{R}$ is defined by $e^\alpha := C \varphi(s_0)^{\beta-1} 2^{\frac{\alpha\beta}{\beta-1}}$, then $\varphi(s_0 + e) = 0$.

Now, we present the main result of this section.

Proposition 2.2. *The unique weak solution u to Problem (2.14) belongs to $L^\infty(\Omega)$. Moreover, there is a positive constant $\bar{e} > 0$, depending only on $d, \Omega, \|l\|_{L^2(\Omega)}, \epsilon_{\min}$, such that $\|u\|_{L^\infty(\Omega)} \leq \|w\|_{L^\infty(\Omega_2)} + \bar{e}$. If $l = 0$, then the constant \bar{e} is equal to zero.*

Proof. To prove the boundedness of u we apply the theorem in [12] once again.

The first step is to show that (2.14) holds for $v = G_s(u) := \text{sgn}(u) \max\{|u| - s, 0\}$ and $s \geq \|w\|_{L^\infty(\Omega_2)}$. Similar test functions G_s have been used in [6, Theorem B.2] in the context of linear elliptic problems.

First, we note that by Stampacchia's theorem (Theorem 2.2.5 in [24]) G_s is Lipschitz continuous with $G_s(0) = 0$ and hence $G_s(u) \in H_0^1(\Omega)$. From $a(u, \cdot) \in H^{-1}(\Omega)$, $(l, \cdot) \in H^{-1}(\Omega)$ and using (2.14) it follows that $b(x, u + w) \in H^{-1}(\Omega) \cap L_{loc}^1(\Omega)$. Then, in view of Brézis and Browder's theorem ([12]), it suffices to show that

$$b(x, u + w)G_s(u) \geq f \text{ a.e. for some } f \in L^1(\Omega). \quad (2.16)$$

Choosing $s \geq \|w\|_{L^\infty(\Omega_2)}$, using the monotonicity of $b(x, \cdot)$, and the fact that $b(x, 0) = 0$, we obtain

$$b(x, u + w)G_s(u) = \begin{cases} b(x, u + w)(u - s) \geq 0 & \text{for } u > s \\ 0 & \text{for } u \in [-s, s] \\ b(x, u + w)(u + s) \geq 0 & \text{for } u < -s, \end{cases} \quad (2.17)$$

which shows the assumption (2.16) for $f = 0$.

Now we are ready to prove that $u \in L^\infty(\Omega)$. First, we consider the case $l = 0$. From (2.17), it follows that

$$\int_{\Omega} b(x, u + w)G_s(u)dx \geq 0. \quad (2.18)$$

Moreover,

$$\begin{aligned} a(u, G_s(u)) &= \int_{\Omega} \epsilon \nabla u \cdot \nabla G_s(u) = \int_{\Omega} \epsilon \nabla G_s(u) \cdot \nabla G_s(u) dx \\ &\geq \epsilon_{\min} \|\nabla G_s(u)\|_{L^2(\Omega)}^2 \geq \frac{\epsilon_{\min}}{C_F^2} \|G_s(u)\|_{L^2(\Omega)}^2, \end{aligned} \quad (2.19)$$

where C_F is the constant in Friedrichs' inequality $\|v\|_{L^2(\Omega)} \leq C_F \|\nabla v\|_{L^2(\Omega)}$ that holds for all $v \in H_0^1(\Omega)$. Finally, using (2.14), (2.18), and (2.19) we get

$$\|G_s(u)\|_{L^2(\Omega)}^2 \leq 0, \text{ for all } s \geq \|w\|_{L^\infty(\Omega_2)}.$$

Consequently $|u| \leq s$ almost everywhere and for all $s \geq \|w\|_{L^\infty(\Omega_2)}$.

In the case where l is not identically zero in Ω , we further estimate $a(u, G_s(u))$ from below and $\int_{\Omega} l G_s(u) dx$ from above using the Sobolev embedding $H^1(\Omega) \hookrightarrow L^q(\Omega)$ where

$q = \infty$ for $d = 1$, $q < \infty$ for $d = 2$, and $q = \frac{2d}{d-2}$ for $d \geq 3$. With q^* we will denote the Hölder conjugate to q . Thus, $q^* = 1$ for $d = 1$, $q^* = \frac{q}{q-1} > 1$ for $d = 2$, and $q^* = \frac{2d}{d+2}$ for $d > 2$. In order to treat both cases in which we are interested simultaneously, namely $d = 2, 3$, we can take $q = 6$ and $q^* = 6/5$. With C_E we denote the embedding constant in the inequality $\|v\|_{L^q(\Omega)} \leq C_E \|v\|_{H^1(\Omega)}$, $\forall v \in H^1(\Omega)$, which depends only on the domain Ω and d . Moreover, we define $A(s) := \{x \in \Omega : |u(x)| > s\}$. For $a(u, G_s(u))$, we have

$$a(u, G_s(u)) = \int_{\Omega} \epsilon \nabla G_s(u) \cdot \nabla G_s(u) dx \geq \frac{\epsilon_{\min}}{1 + C_F^2} \|G_s(u)\|_{H^1(\Omega)}^2 \quad (2.20)$$

and for $\int_{\Omega} l G_s(u) dx$ we obtain

$$\begin{aligned} \int_{\Omega} l G_s(u) dx &= \int_{A(s)} l G_s(u) dx \leq \|l\|_{L^{q^*}(A(s))} \|G_s(u)\|_{L^q(\Omega)} \\ &\leq C_E \|l\|_{L^{q^*}(A(s))} \|G_s(u)\|_{H^1(\Omega)}. \end{aligned} \quad (2.21)$$

Combining (2.20), (2.21), (2.18), and (2.14), we obtain

$$\frac{\epsilon_{\min}}{1 + C_F^2} \|G_s(u)\|_{H^1(\Omega)} \leq C_E \|l\|_{L^{q^*}(A(s))}. \quad (2.22)$$

The final step before applying Lemma 2.1 is to estimate the left-hand side of (2.22) from below in terms of $|A(h)|$ for $h > s \geq \|w\|_{L^\infty(\Omega_2)}$ and the right-hand side of (2.22) from above in terms of $|A(s)|$. Again using the Sobolev embedding $H^1(\Omega) \hookrightarrow L^q(\Omega)$ and Hölder's inequality yields

$$\begin{aligned} \|G_s(u)\|_{H^1(\Omega)} &\geq \frac{1}{C_E} \left(\int_{\Omega} |G_s(u)|^q dx \right)^{\frac{1}{q}} = \frac{1}{C_E} \left(\int_{A(s)} |u|^{-s} dx \right)^{\frac{1}{q}} \\ &\geq \frac{1}{C_E} \left(\int_{A(h)} (h-s)^q dx \right)^{\frac{1}{q}} = \frac{1}{C_E} (h-s) |A(h)|^{\frac{1}{q}} \end{aligned} \quad (2.23)$$

and

$$\|l\|_{L^{q^*}(A(s))} \leq \|l\|_{L^2(\Omega)} |A(s)|^{\frac{2-q^*}{2q^*}}. \quad (2.24)$$

Combining (2.23), (2.24), and (2.22), we obtain the following inequality for the nonnegative and nonincreasing function $\varphi(t) := |A(t)|$

$$|A(h)| \leq \left(\frac{C_E^2 (1 + C_F^2)}{\epsilon_{\min}} \|l\|_{L^2(\Omega)} \right)^q \frac{|A(s)|^{\frac{q-2}{2}}}{(h-s)^q}, \quad \text{for all } h > s \geq \|w\|_{L^\infty(\Omega_2)}. \quad (2.25)$$

Since $\frac{q-2}{q} = 2 > 1$, by applying Lemma 2.1 we conclude that there is some $e > 0$ such that

$$\begin{aligned} 0 < e^q &= \left(\frac{C_E^2 (1 + C_F^2)}{\epsilon_{\min}} \|l\|_{L^2(\Omega)} \right)^q |A(\|w\|_{L^\infty(\Omega_2)})|^{\frac{q-4}{2}} 2^{\frac{q(q-2)}{q-4}} \\ &\leq \left(\frac{C_E^2 (1 + C_F^2)}{\epsilon_{\min}} \|l\|_{L^2(\Omega)} \right)^q |\Omega|^{\frac{q-4}{2}} 2^{\frac{q(q-2)}{q-4}} =: \bar{e}^q \end{aligned}$$

and $|A(\|w\|_{L^\infty(\Omega_2)} + \bar{e})| = 0$. Hence $\|u\|_{L^\infty(\Omega)} \leq \|w\|_{L^\infty(\Omega_2)} + \bar{e}$. \square

Remark 2.2. *Since $k = 0$ in Ω_1 , $w \in L^\infty(\Omega_2)$ and $u \in L^\infty(\Omega)$, we conclude that (2.14) holds for all $v \in H_0^1(\Omega)$ resulting in a standard weak formulation. If k^2 is uniformly positive in the whole domain Ω and $w \in L^\infty(\Omega)$, then we have that $\|u\|_{L^\infty(\Omega)} \leq \|w\|_{L^\infty(\Omega)} + \bar{e}$. On the other hand, if $k = 0$ in Ω_2 , k^2 is uniformly positive in Ω_1 , and $w \in L^\infty(\Omega_1)$, we have $\|u\|_{L^\infty(\Omega)} \leq \|w\|_{L^\infty(\Omega_1)} + \bar{e}$.*

3 A posteriori error estimates

We set $V := H_0^1(\Omega)$, $Y := [L^2(\Omega)]^d$ ($d = 2, 3$), and Λ the gradient operator $\nabla : H_0^1(\Omega) \rightarrow [L^2(\Omega)]^d$. We further denote $g : \Omega \times \mathbb{R}^3 \rightarrow \mathbb{R}$, $g(x, \xi) := \frac{\epsilon(x)}{2} |\xi|^2$, and $B : \Omega \times \mathbb{R} \rightarrow \mathbb{R}$, $B(x, \xi) := k^2(x) \cosh(\xi)$. With this notation, we have

$$\begin{aligned} G(\Lambda v) &:= \int_{\Omega} g(x, \nabla v(x)) dx = \int_{\Omega} \frac{\epsilon}{2} |\nabla v|^2 dx, \\ F(v) &:= \int_{\Omega} B(x, v(x) + w(x)) dx = \int_{\Omega} k^2 \cosh(v + w) dx - \int_{\Omega} l v dx. \end{aligned}$$

For any $v \in V$ the functional $G(\Lambda v)$ is finite, while $F : V \rightarrow \mathbb{R} \cup \{+\infty\}$ may take the value $+\infty$ for some $v \in V$ if $d \geq 3$ (e.g $v = \log \frac{1}{|x|^\alpha}$, $\alpha \geq d$ on the unit ball in \mathbb{R}^d). However, if $d \leq 2$, then $\exp(v) \in L^1(\Omega)$, $\forall v \in H_0^1(\Omega)$ and $F : V \rightarrow \mathbb{R}$ (see [2]). Also, $F(0_V)$ is obviously finite since $w \in L^\infty(\Omega_2)$. We set $V^* = H^{-1}(\Omega)$ and $Y^* = Y = [L^2(\Omega)]^d$. In this case, Λ^* coincides with $-\operatorname{div}$ considered as an operator from $[L^2(\Omega)]^d$ to $H^{-1}(\Omega)$. First we will give an explicit form of the error estimate in terms of forcing functionals using (2.7) and then we will present the particular form of the error equality (2.11) where the error is measured in a special "nonlinear norm". This measure contains the usual combined energy norm terms, i.e. the sum of the energy norms of the errors for the primal and dual problem, but also two additional nonnegative terms due to the nonlinearity $B(x, \xi)$ (or equivalently $b(x, \xi)$) which in some cases may dominate the usual energy norm terms. We start by deriving explicit expressions for G^* , F^* , Υ_G , Υ_{G^*} , Υ_F , Υ_{F^*} and then we will use these expressions to get an explicit form of the abstract error estimates (2.7) and (2.11).

3.1 Fenchel Conjugates of G and F

It is easy to find that $G^*(y^*) = \int_{\Omega} \frac{1}{2\epsilon(x)} |y^*(x)|^2 dx$. For $y^* \in H(\operatorname{div}; \Omega)$ and an arbitrary function $z : \Omega_2 \rightarrow \mathbb{R}$, we introduce

$$I_{y^*}(z) := \int_{\Omega_2} [(\operatorname{div} y^* + l)z - B(x, z + w)] dx. \quad (3.1)$$

Recalling that the nonlinearity B is supported on Ω_2 , we have

$$\begin{aligned} F^*(-\Lambda^* y^*) &= \sup_{z \in H_0^1(\Omega)} [\langle -\Lambda^* y^*, z \rangle - F(z)] = \sup_{z \in H_0^1(\Omega)} [(-y^*, \Lambda z) - F(z)] \\ &= \sup_{z \in H_0^1(\Omega)} \int_{\Omega} [-y^* \cdot \nabla z - B(x, z + w) + lz] dx = \quad (\text{if } y^* \in H(\operatorname{div}; \Omega)) \\ &= \sup_{z \in H_0^1(\Omega)} \int_{\Omega} [\operatorname{div} y^* z - B(x, z + w) + lz] dx \quad (\text{finite if } \operatorname{div} y^* + l = 0 \text{ in } \Omega_1) \\ &= \sup_{z \in H_0^1(\Omega)} I_{y^*}(z) \leq \int_{\Omega_2} \sup_{\xi \in \mathbb{R}} [(\operatorname{div} y^*(x) + l(x)) \xi - B(x, \xi + w(x))] dx \\ &= \int_{\Omega_2} [(\operatorname{div} y^*(x) + l(x)) \xi_0(x) - B(x, \xi_0(x) + w(x))] dx = I_{y^*}(\xi_0). \end{aligned} \quad (3.2)$$

Here $\xi_0 : \Omega_2 \rightarrow \mathbb{R}$ is computed from the condition

$$\frac{d}{d\xi} [(\operatorname{div} y^*(x) + l(x)) \xi - B(x, \xi + w(x))] = 0, \quad \text{for a.e. } x \in \Omega_2, \quad (3.3)$$

which is equivalent to

$$\operatorname{div} y^*(x) + l(x) - k^2(x) \sinh(\xi + w(x)) = 0 \quad \text{for a.e. } x \in \Omega_2.$$

We notice that (3.3) is a necessary condition for a maximum which is also sufficient since $B(x, \cdot)$ is convex. The solution of the last equation exists, is unique, and is given by

$$\begin{aligned} \xi_0(x) &= \operatorname{arsinh}(\rho_k(y^*)) - w(x) \\ &= \ln \left(\rho_k(y^*) + \sqrt{\rho_k^2(y^*) + 1} \right) - w(x) = \ln(\Theta(\rho_k(y^*))) - w(x), \end{aligned} \quad (3.4)$$

where $\rho_k(y^*) := \frac{\operatorname{div} y^*(x) + l(x)}{k^2(x)}$ and $\Theta(s) := s + \sqrt{s^2 + 1}$ for $s \in \mathbb{R}$. Note that the exact solution $p^* = \epsilon \nabla u$ of the dual Problem (P^*) also satisfies the relation $\operatorname{div}(\epsilon \nabla u) + l = 0$ because for any $x \in \Omega_1$ it holds $k(x) = 0$. Moreover, since $u \in L^\infty(\Omega)$, $w \in L^\infty(\Omega_2)$, and $l \in L^2(\Omega)$, we see that the $\operatorname{div} p^* = k^2 \sinh(u + w) + l \in L^2(\Omega)$ and thus $p^* \in H(\operatorname{div}; \Omega)$. In Proposition 3.1, we will later prove that we have not overestimated the supremum over $z \in H_0^1(\Omega)$ in (3.2) and that we actually have equalities everywhere. Denoting $S := \operatorname{arsinh}(\rho_k(y^*))$, and using the expression for $\xi_0(x)$ and the formula $\cosh(\operatorname{arsinh}(x)) = \sqrt{x^2 + 1}$, $\forall x \in \mathbb{R}$, for any $y^* \in H(\operatorname{div}; \Omega) \subset [L^2(\Omega)]^d = Y^*$ with $\operatorname{div} y^* + l = 0$ in Ω_1 we obtain an explicit formula for $F^*(-\Lambda^* y^*)$:

$$\begin{aligned} F^*(-\Lambda^* y^*) &= \int_{\Omega_2} \left[k^2 \rho_k(y^*) (\ln(\Theta(\rho_k(y^*))) - w) - k^2 \sqrt{\rho_k^2(y^*) + 1} \right] dx \\ &= \int_{\Omega_2} \left[k^2 \sinh(S)(S - w) - k^2 \cosh(S) \right] dx \end{aligned} \quad (3.5)$$

Remark 3.1. *Since $|\ln(t + \sqrt{t^2 + 1})| \leq |t|$, $\forall t \in \mathbb{R}$, the function $\ln(\Theta(f(x))) - w(x)$ belongs to $L^2(\Omega_2)$ for any $f \in L^2(\Omega_2)$ and we conclude that $\xi_0(x) \in L^2(\Omega_2)$ if $y^* \in H(\operatorname{div}; \Omega)$. Therefore the integral in (3.5) is well defined.*

Now our goal is to prove that the inequality $\sup_{z \in H_0^1(\Omega)} I_{y^*}(z) \leq I_{y^*}(\xi_0)$ holds as the equality. In other words, we want to prove that the error estimate remains sharp and that the computed majorant $M_{\oplus}^2(v, y^*)$ will be indeed zero if approximations (v, y^*) coincide with the exact solution (u, p^*) .

Proposition 3.1. *For any $y^* \in H(\operatorname{div}; \Omega)$ with $\operatorname{div} y^* + l = 0$ in Ω_1 it holds*

$$\sup_{z \in H_0^1(\Omega)} I_{y^*}(z) = I_{y^*}(\xi_0) < \infty.$$

Proof. The idea is to approximate $f = \frac{\operatorname{div} y^* + l}{k^2} \in L^2(\Omega_2)$ and $w|_{\Omega_2} \in L^\infty(\Omega_2)$ by $C_0^\infty(\Omega_2)$ functions (in the a.e. sense) and use the Lebesgue dominated convergence theorem. Let $f_n \in C_0^\infty(\Omega_2)$ and $w_n \in C_0^\infty(\Omega_2)$ be such that $f_n(x) \rightarrow f(x)$, a.e. in Ω_2 , $|f_n(x)| \leq h(x) \in L^2(\Omega_2)$ (see Theorem 4.9 in [11]), $w_n(x) \rightarrow w(x)$, a.e. in Ω_2 , $|w_n(x)| \leq m + 2$, where $m := \|w\|_{L^\infty(\Omega_2)}$. Then $z_n(x) := \ln(\Theta(f_n(x))) - w_n(x) \rightarrow \xi_0(x)$, a.e. in Ω_2 and $z_n \in C_0^\infty(\Omega_2) \subset H_0^1(\Omega_2) \subset H_0^1(\Omega)$ (by extending the functions by zero in Ω_1). Since $B(x, \cdot)$ is continuous, we have the pointwise a.e. in Ω_2 convergence

$$(\operatorname{div} y^*(x) + l(x)) z_n(x) - B(x, z_n + w(x)) \rightarrow (\operatorname{div} y^*(x) + l(x)) \xi_0(x) - B(x, \xi_0(x) + w(x))$$

Now we search for a function in $L^1(\Omega_2)$ that majorates the function $|(\operatorname{div} y^*(x) + l(x)) z_n(x) - B(x, z_n + w(x))|$:

$$\begin{aligned} &|(\operatorname{div} y^*(x) + l(x)) z_n(x) - k^2(x) \cosh(z_n(x) + w(x))| \\ &\leq |\operatorname{div} y^*(x) + l(x)| |z_n(x)| + k^2(x) e^{\|w\|_{L^\infty(\Omega_2)}} e^{|z_n(x)|} \end{aligned} \quad (3.6)$$

Our next goal is to bound $|z_n(x)|$ in (3.6). For the first summand, we have

$$|z_n(x)| = |\ln(\Theta(f_n(x))) - w_n(x)| \leq |f_n(x)| + m + 2 \leq h(x) + m + 2 \in L^2(\Omega_2)$$

where Remark 3.1 has been used. However, this bound cannot be used in the second term because e^h might not belong even to $L^1(\Omega_2)$. In order to find an L^1 -majorant for the second summand in (3.6), we distinguish the following two cases:

In the first case $f_n(x) > 0$. Then $|\ln(\Theta(f_n(x)))| \leq |\ln(\Theta(h(x)))|$.

In the second case ($f_n(x) \leq 0$), we have $\Theta(f_n(x)) \leq 1$. Therefore, $0 \geq f_n(x) \geq -h(x)$. Since $\Theta(s)$ is a monotonically increasing function,

$$\Theta(0) = 1 \geq \Theta(f_n(x)) \geq \Theta(-h(x)) > 0.$$

From here we obtain

$$\ln(1) = 0 \geq \ln(\Theta(f_n(x))) \geq \ln(\Theta(-h(x)))$$

and using the relation $\Theta(-h) = \frac{1}{\Theta(h)}$ we conclude that

$$|\ln(\Theta(f_n(x)))| \leq |\ln(\Theta(-h(x)))| = |\ln(\Theta(h(x)))|.$$

Finally, for almost all $x \in \Omega_2$ we have

$$\begin{aligned} |z_n(x)| &= |\ln(\Theta(f_n(x))) - w_n(x)| \leq |\ln(\Theta(h(x)))| + m + 2 \\ &= \ln(\Theta(h(x))) + m + 2, \text{ because } h(x) \geq 0, \text{ for a.e. } x \in \Omega_2. \end{aligned}$$

Therefore,

$$\begin{aligned} &|(\operatorname{div} y^*(x) + l(x)) z_n(x) - k^2(x) \cosh(z_n(x) + w(x))| \\ &\leq |\operatorname{div} y^*(x) + l(x)| (h(x) + \|w\|_{L^\infty(\Omega_2)} + 2) \\ &+ k^2(x) e^{2\|w\|_{L^\infty(\Omega_2)} + 2} \Theta(h(x)) := H(x) \in L^2(\Omega_2), \end{aligned}$$

where in the last line we used the fact that $\Theta(h(x)) \in L^2(\Omega_2)$. All the conditions of the Lebesgue's dominated convergence theorem are satisfied and we see that $I_{y^*}(z_n) \rightarrow I_{y^*}(\xi_0)$ and, consequently, $\sup_{z \in H_0^1(\Omega)} I_{y^*}(z) = I_{y^*}(\xi_0)$. \square

3.2 Forcing Functionals

Now our goal is to compute the forcing functionals $\Upsilon_G, \Upsilon_{G^*}, \Upsilon_F, \Upsilon_{F^*}$. For any $y_1, y_2 \in Y = [L^2(\Omega)]^d$, we have

$$\begin{aligned} \frac{1}{2}G(y_1) + \frac{1}{2}G(y_2) - G\left(\frac{y_1 + y_2}{2}\right) &= \frac{1}{2} \int_{\Omega} \frac{\epsilon}{2} |y_1|^2 dx + \frac{1}{2} \int_{\Omega} \frac{\epsilon}{2} |y_2|^2 dx - \int_{\Omega} \frac{\epsilon}{2} \left(\frac{y_1 + y_2}{2}\right)^2 dx \\ &= \frac{1}{8} \int_{\Omega} \epsilon |y_1 - y_2|^2 dx =: \Upsilon_G(y_1 - y_2). \end{aligned} \quad (3.7)$$

Similarly, for any $y_1^*, y_2^* \in Y^* = [L^2(\Omega)]^d$ we get

$$\Upsilon_{G^*}(y_1^* - y_2^*) = \frac{1}{8} \int_{\Omega} \frac{1}{\epsilon} |y_1^* - y_2^*|^2 dx. \quad (3.8)$$

We note that according to the definition of uniformly convex functional, F is not uniformly convex because $k = 0$ in Ω_1 and therefore F is affine on the linear subspace $H_0^1(\Omega_m) \subset H_0^1(\Omega) = V$, where functions in $H_0^1(\Omega_1)$ are extended by zero into Ω_2 . Thus, if there is a nonnegative functional Υ_F such that (2.2) is satisfied for all $v_1, v_2 \in V$, it will be necessarily zero for all v_1, v_2 such that $v_1 = v_2$ in Ω_2 (see Remark 2.1). If F_1 is uniformly convex with forcing functional Υ_{F_1} and F_2 is convex, then $F = F_1 + F_2$ is uniformly convex

with a forcing functional $\Upsilon_F = \Upsilon_{F_1}$. Since $F(v) = \int_{\Omega} B(x, v + w) dx - \int_{\Omega} l v dx$ it is enough to find a forcing functional $\Upsilon_{\tilde{B}_x} : \mathbb{R} \rightarrow \mathbb{R}$ for $\tilde{B}_x(\cdot) := B(x, \cdot + w(x)) : \mathbb{R} \rightarrow \mathbb{R}$ for a.e. $x \in \Omega$. In this case, we will define $\Upsilon_F(v_1 - v_2) := \int_{\Omega} \Upsilon_{\tilde{B}_x}(v_1 - v_2) dx$. We need to find $\Upsilon_{\tilde{B}_x}$ such that

$$\Upsilon_{\tilde{B}_x}(\xi_1 - \xi_2) \leq \frac{1}{2} \tilde{B}_x(\xi_1) + \frac{1}{2} \tilde{B}_x(\xi_2) - \tilde{B}_x\left(\frac{\xi_1 + \xi_2}{2}\right), \forall \xi_1, \xi_2 \in \mathbb{R}. \quad (3.9)$$

If we denote $\zeta := \xi_1 - \xi_2$ then $\xi_2 = \xi_1 - \zeta$ and we have

$$\Upsilon_{\tilde{B}_x}(\zeta) \leq \frac{1}{2} \tilde{B}_x(\xi_1) + \frac{1}{2} \tilde{B}_x(\xi_1 - \zeta) - \tilde{B}_x\left(\frac{2\xi_1 - \zeta}{2}\right), \forall \xi_1, \zeta \in \mathbb{R}.$$

Thus, we define

$$\begin{aligned} \Upsilon_{\tilde{B}_x}(\zeta) &:= \inf_{\xi_1 \in \mathbb{R}} \left[\frac{1}{2} \tilde{B}_x(\xi_1) + \frac{1}{2} \tilde{B}_x(\xi_1 - \zeta) - \tilde{B}_x\left(\frac{2\xi_1 - \zeta}{2}\right) \right] \\ &= \inf_{\xi_1 \in \mathbb{R}} \left[\frac{k^2(x)}{2} \left(\cosh(\xi_1 + w(x)) + \cosh(\xi_1 - \zeta + w(x)) - 2 \cosh\left(\frac{2\xi_1 - \zeta}{2} + w(x)\right) \right) \right]. \end{aligned}$$

A necessary condition for $\bar{\xi}_1$ to minimize the above expression is that the first derivative with respect to ξ_1 vanishes at $\bar{\xi}_1$, i.e.,

$$\begin{aligned} \frac{d}{d\xi_1} \left[\frac{k^2(x)}{2} \left(\cosh(\xi_1 + w(x)) + \cosh(\xi_1 - \zeta + w(x)) \right. \right. \\ \left. \left. - 2 \cosh\left(\frac{2\xi_1 - \zeta}{2} + w(x)\right) \right) \right] = 0. \end{aligned} \quad (3.10)$$

Since the second derivative with respect to ξ_1 is always positive because of the convexity of \cosh , we see that the necessary condition for a minimum is also a sufficient condition. After using the formula $\sinh(\xi) = \frac{\exp(\xi) - \exp(-\xi)}{2}$ and making the substitutions $\exp(\xi_1 + w(x)) = r > 0$ and $\exp(\zeta/2) = a > 0$ in (3.10) we get

$$\frac{1}{2} \left(r - \frac{1}{r} \right) + \frac{1}{2} \left(\frac{r}{a^2} - \frac{a^2}{r} \right) - \left(\frac{r}{a} - \frac{a}{r} \right) = 0$$

from which after solving for r we get $r = a$ and $\bar{\xi}_1(x) = \frac{\zeta}{2} - w(x)$. Therefore,

$$\Upsilon_{\tilde{B}_x}(\zeta) = k^2(x) \left[\cosh\left(\frac{\zeta}{2}\right) - 1 \right] \quad (3.11)$$

and thus

$$\Upsilon_F(v - u) = \int_{\Omega} k^2 \left[\cosh\left(\frac{v - u}{2}\right) - 1 \right] dx. \quad (3.12)$$

Here we note that

$$\Upsilon_F(v - u) \geq \int_{\Omega} \frac{k^2}{8} (v - u)^2 dx := \underline{\Upsilon}_F(v - u) \quad (3.13)$$

since $\cosh\left(\frac{\xi}{2}\right) - 1 \geq \frac{\xi^2}{8}$, $\forall \xi \in \mathbb{R}$ and thus $\underline{\Upsilon}_F$ is also a forcing functional (see Figure 1). If k^2 is uniformly positive on the whole domain Ω , then $\sqrt{\underline{\Upsilon}_F(v - u)}$ is equivalent to the

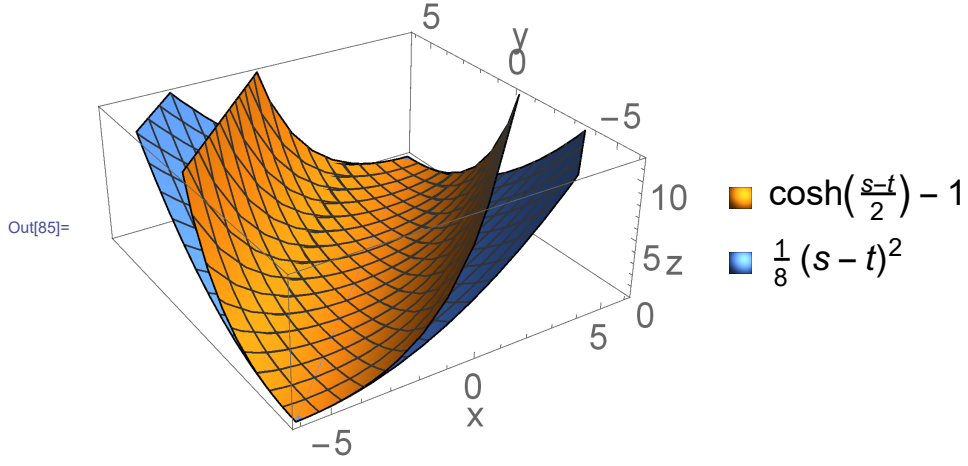


Figure 1: Lower bound of $\cosh\left(\frac{s-t}{2}\right) - 1$ formed by a quadratic function.

$L^2(\Omega)$ norm of $v - u$. Finally, we obtain a forcing functional for F^* . We have derived an explicit expression for F^* only for arguments of the form $-\Lambda^* y^*$ where $y^* \in H(\text{div}; \Omega) \subset [L^2(\Omega)]^d = Y^*$. Therefore, we will search only for a forcing functional Υ_{F^*} which takes such arguments, i.e. $F^*(-\Lambda^* y^* + \Lambda^* p^*)$. We should also note that these arguments are abstract elements from the dual space of $H_0^1(\Omega)$. However (as we already saw in (3.2)), if $y^* \in H(\text{div}; \Omega)$, then

$$\begin{aligned}
F^*(-\Lambda^* y^*) &= \sup_{z \in H_0^1(\Omega)} \int_{\Omega} [\text{div } y^* z - B(x, z + w) + lz] dx \\
&= \sup_{z \in L^2(\Omega)} \int_{\Omega} [\text{div } y^* z - B(x, z + w) + lz] dx \\
&=: \tilde{F}^*(\text{div } y^*)
\end{aligned} \tag{3.14}$$

where \tilde{F}^* is the Fenchel conjugate of the functional $\tilde{F} : L^2(\Omega) \rightarrow \mathbb{R} \cup \{+\infty\}$ defined by

$$\tilde{F}(z) = \int_{\Omega} [B(x, z + w) - lz] dx, \forall z \in L^2(\Omega)$$

and the supremum over $z \in H_0^1(\Omega)$ is equal to the supremum over $z \in L^2(\Omega)$ due to Remark 3.1 and Proposition 3.1¹. Thus, for all $y^* \in H(\text{div}; \Omega)$ we have

$$F^*(-\Lambda^* y^*) = \tilde{F}^*(\text{div } y^*) \tag{3.15}$$

and additionally $\tilde{F}^*(\text{div } y^*)$ is equal to the expression in (3.5):

$$\tilde{F}^*(\text{div } y^*) = I_{y^*}(\xi_0) =: \int_{\Omega_2} f_x^*(\text{div } y^*) dx$$

where $f_x^* : \mathbb{R} \rightarrow \mathbb{R}$ and for a.e. $x \in \Omega_2$ and for all $r \in \mathbb{R}$

$$f_x^*(r) = (r + l(x)) \left(\text{arsinh} \left(\frac{r + l(x)}{k^2(x)} \right) - w(x) \right) - k^2(x) \cosh \left(\text{arsinh} \left(\frac{r + l(x)}{k^2(x)} \right) \right).$$

¹Note that the functional $(\text{div } y^*, z) - \tilde{F}(z)$ is only upper semicontinuous and is not continuous over $L^2(\Omega)$ and thus we cannot use a density argument to prove that both suprema are equal.

If $\Upsilon_{\tilde{F}^*}$ is a forcing functional for \tilde{F}^* , then we have

$$\tilde{F}^* \left(\frac{\operatorname{div} y^* - \operatorname{div} p^*}{2} \right) + \Upsilon_{\tilde{F}^*}(\operatorname{div} y^* - \operatorname{div} p^*) \leq \frac{1}{2} \tilde{F}^*(\operatorname{div} y^*) + \frac{1}{2} \tilde{F}^*(\operatorname{div} p^*),$$

which due to (3.15) is exactly the same as

$$F^* \left(\frac{-\Lambda^* y^* + \Lambda^* p^*}{2} \right) + \Upsilon_{F^*}(-\Lambda^* y^* + \Lambda^* p^*) \leq \frac{1}{2} F^*(-\Lambda^* y^*) + \frac{1}{2} F^*(-\Lambda^* p^*).$$

Here $\Upsilon_{F^*}(-\Lambda^*(y^* - p^*)) := \Upsilon_{\tilde{F}^*}(\operatorname{div}(y^* - p^*))$, $\forall y^*, p^* \in H(\operatorname{div}; \Omega)$. With this remark, it is clear that we only need to find the forcing functional $\Upsilon_{\tilde{F}^*} : L^2(\Omega) \supset \operatorname{R}(\operatorname{div}) \rightarrow \overline{\mathbb{R}}$ where $\operatorname{R}(\operatorname{div})$ is the range of the divergence operator as an operator from $[L^2(\Omega)]^d$ to $L^2(\Omega)$. Again, since \tilde{F}^* is an integral functional, i.e. $\tilde{F}^*(\operatorname{div} y^*) = \int_{\Omega_2} f_x^*(\operatorname{div} y^*) dx$ it is enough to

find a forcing functional $\Upsilon_{f_x^*} : \mathbb{R} \rightarrow \mathbb{R}$ for f_x^* .

For any $\xi_1, \xi_2 \in \mathbb{R}$ it holds

$$\Upsilon_{f_x^*}(\xi_1 - \xi_2) \leq \frac{1}{2} f_x^*(\xi_1) + \frac{1}{2} f_x^*(\xi_2) - f_x^* \left(\frac{\xi_1 + \xi_2}{2} \right).$$

Since $f_x^*(r) =: h_x^*(r + l(x))$, where

$$h_x^*(r) = r \left(\operatorname{arsinh} \left(\frac{r}{k^2(x)} \right) - w(x) \right) - k^2(x) \cosh \left(\operatorname{arsinh} \left(\frac{r}{k^2(x)} \right) \right), \forall r \in \mathbb{R},$$

it suffices to find a forcing functional $\Upsilon_{h_x^*}$ for $h_x^*(r)$ and then define $\Upsilon_{f_x^*}(\zeta) = \Upsilon_{h_x^*}(\zeta)$, $\forall \zeta \in \mathbb{R}$. Again, we make the substitution $\zeta = \xi_1 - \xi_2$. We have

$$\inf_{\xi_1 \in \mathbb{R}} \left[\frac{1}{2} h_x^*(\xi_1) + \frac{1}{2} h_x^*(\xi_1 - \zeta) - h_x^* \left(\frac{2\xi_1 - \zeta}{2} \right) \right] = 0, \forall \zeta \in \mathbb{R}.$$

This means that the function h_x^* is not uniformly convex over \mathbb{R} . However, if we restrict ξ_1, ξ_2 to a ball $B(0, \delta) \subset \mathbb{R}^2$, $\delta > 0$, then the above infimum is greater than zero, and according to the definition of uniform convexity, h_x^* will be uniformly convex over the ball $B(0, \delta)$. This can be useful in the context of our particular problem when $l \in L^\infty(\Omega_2)$, since from Proposition 2.2 we have that $\operatorname{div}(\epsilon \nabla u) + l = \operatorname{div} p^* + l = k^2 \sinh(u + w) \in L^\infty(\Omega_2)$. Therefore, if we pick the approximations $y^* \in H(\operatorname{div}; \Omega)$ for the solution p^* of the dual Problem (P^*) with $\operatorname{div} y^* + l = 0$ in Ω_1 and additionally such that $\operatorname{div} y^* + l \in L^\infty(\Omega_2)$ with $-M \leq \operatorname{div} y^* + l \leq M$ for some $M > 0$, then for almost each $x \in \Omega_2$

$$\begin{aligned} & - \|k^2\|_{L^\infty(\Omega_2)} \sinh(2\|w\|_{L^\infty(\Omega_2)} + \bar{e}) \leq \operatorname{div} p^* + l \leq \|k^2\|_{L^\infty(\Omega_2)} \sinh(2\|w\|_{L^\infty(\Omega_2)} + \bar{e}), \\ & - \|k^2\|_{L^\infty(\Omega_2)} \sinh(2\|w\|_{L^\infty(\Omega_2)} + \bar{e}) - M \leq \operatorname{div} y^* - \operatorname{div} p^* \\ & \leq \|k^2\|_{L^\infty(\Omega_2)} \sinh(2\|w\|_{L^\infty(\Omega_2)} + \bar{e}) + M, \end{aligned}$$

and thus we can choose $\delta = \max \{ \|k^2\|_{L^\infty(\Omega_2)} \sinh(2\|w\|_{L^\infty(\Omega_2)} + \bar{e}), M \}$ and $B(0, \delta) = [-\delta, \delta]^2$ in \mathbb{R}^2 . In this case, for any $-2\delta \leq \zeta \leq 2\delta$

$$\Upsilon_{h_x^*}(\zeta) = \inf_{-\delta \leq \xi_1 \leq \delta} \left[\frac{1}{2} h_x^*(\xi_1) + \frac{1}{2} h_x^*(\xi_1 - \zeta) - h_x^* \left(\frac{2\xi_1 - \zeta}{2} \right) \right] > 0.$$

Now, depending on k and the above defined δ , one can find a constant C_1 such that for all $\xi_1 \in [-\delta, \delta]$ and $\zeta \in [-2\delta, 2\delta]$ the following inequality is satisfied

$$C_1 \zeta^2 \leq \frac{1}{2} h_x^*(\xi_1) + \frac{1}{2} h_x^*(\xi_1 - \zeta) - h_x^* \left(\frac{2\xi_1 - \zeta}{2} \right).$$

This means that we can define $\Upsilon_{f_x^*}(\zeta) = \Upsilon_{h_x^*}(\zeta) = C_1\zeta^2$ and consequently the forcing functional Υ_{F^*} as follows

$$\begin{aligned}\Upsilon_{F^*}(-\Lambda^*y^* + \Lambda^*p^*) &= \Upsilon_{\tilde{F}^*}(\operatorname{div} y^* - \operatorname{div} p^*) \\ &= \int_{\Omega_2} \Upsilon_{f_x^*}(\operatorname{div} y^* - \operatorname{div} p^*) dx = \int_{\Omega_2} C_1(\operatorname{div} y^* - \operatorname{div} p^*)^2 dx.\end{aligned}\quad (3.16)$$

3.3 Error measures

In this section, we apply the abstract framework from Section 2 and derive explicit forms of relations (2.7) and (2.11) adapted to our problem. Using (3.13) and (3.16), for any $v \in H_0^1(\Omega)$ and $y^* \in Y_M^*$, where

$$Y_M^* := \{y^* \in H(\operatorname{div}; \Omega), \text{ s.t. } \operatorname{div} y^* + l = 0 \text{ in } \Omega_1 \text{ and } -M \leq \operatorname{div} y^* + l \leq M \text{ in } \Omega_2\},$$

the estimate (2.7) takes the form

$$\begin{aligned}&\frac{1}{8} \int_{\Omega} \epsilon |\nabla(v - u)|^2 dx + \frac{1}{8} \int_{\Omega} \frac{1}{\epsilon} |y^* - p^*|^2 dx + \frac{1}{8} \int_{\Omega} k^2 (v - u)^2 dx + C_1 \int_{\Omega} |\operatorname{div} y^* - \operatorname{div} p^*|^2 dx \\ &\leq \frac{1}{8} \int_{\Omega} \epsilon |\nabla(v - u)|^2 dx + \frac{1}{8} \int_{\Omega} \frac{1}{\epsilon} |y^* - p^*|^2 dx \\ &+ \int_{\Omega} k^2 \left[\cosh\left(\frac{v - u}{2}\right) - 1 \right] dx + C_1 \int_{\Omega} |\operatorname{div} y^* - \operatorname{div} p^*|^2 dx \leq \frac{1}{2} M_{\oplus}^2(v, y^*),\end{aligned}\quad (3.17)$$

where the constant C_1 depends on k , $\|w\|_{L^\infty(\Omega_2)}$, \bar{e} , and M . The quantity $M_{\oplus}^2(v, y^*)$ is fully computable and is given by the relation

$$\begin{aligned}M_{\oplus}^2(v, y^*) &= D_G(\Lambda v, y^*) + D_F(v, -\Lambda^* y^*) \\ &= G(\Lambda v) + G^*(y^*) - \langle y^*, \Lambda v \rangle + F(v) + F^*(-\Lambda^* y^*) + \langle \Lambda^* y^*, v \rangle \\ &= \int_{\Omega} \eta^2(x) dx = \frac{1}{2} \|\epsilon \nabla v - y^*\|_*^2 + D_F(v, -\Lambda^* y^*),\end{aligned}\quad (3.18)$$

where

$$\eta^2(x) = \begin{cases} \frac{1}{2\epsilon} |\epsilon \nabla v - y^*|^2, & x \in \Omega_1 \\ \frac{1}{2\epsilon} |\epsilon \nabla v - y^*|^2 + k^2 \cosh(v + w) - lv \\ + k^2 \rho_k(y^*) (\ln(\Theta(\rho_k(y^*))) - w) - k^2 \sqrt{\rho_k^2(y^*) + 1} - \operatorname{div} y^* v, & x \in \Omega_2 \end{cases}\quad (3.19)$$

It is clear that $\eta^2(x) \geq 0$ since it is the sum of the compound functionals generated by $\tilde{g}_x(s) := g(x, s)$ and $\tilde{B}_x(s) - l(x)s = B(x, s + w(x)) - l(x)s$ evaluated at $(\nabla v(x), y^*(x))$ and $(v(x), \operatorname{div} y^*(x))$ respectively. It therefore qualifies as an error indicator, provided that y^* is chosen appropriately, which we demonstrate with numerical experiments in the next section. One can also work with the space $Y_\infty^* := \{y^* \in H(\operatorname{div}; \Omega) \text{ s.t. } \operatorname{div} y^* + l = 0 \text{ in } \Omega_2\}$ instead of Y_M^* . In this case, F^* does not possess a nonzero forcing functional and we skip the term with C_1 in (3.17).

Using the expression for G^* , we obtain

$$D_G(\Lambda v, p^*) = \frac{1}{2} \int_{\Omega} \epsilon |\nabla(v - u)|^2 dx =: \frac{1}{2} \|\nabla(v - u)\|^2\quad (3.20)$$

and

$$D_G(\Lambda u, y^*) = \frac{1}{2} \int_{\Omega} \frac{1}{\epsilon} |y^* - p^*|^2 dx =: \frac{1}{2} \| \| y^* - p^* \| \|_*^2. \quad (3.21)$$

Now, we find explicit expressions for the nonlinear measures $D_F(v, -\Lambda^* p^*)$ and $D_F(u, -\Lambda^* y^*)$ similar to the ones for the case of quadratic F in (2.12) for the linear elliptic equation $-\operatorname{div}(A\nabla u) + u = l$. First, we prove the following assertion:

Proposition 3.2. *For all $s, t \in \mathbb{R}$ it holds*

$$\frac{(t-s)^2}{2} \leq A(s, t) \leq \frac{(\sinh(t) - \sinh(s))^2}{2}, \quad (3.22)$$

where $A(s, t) = \cosh(t) - \cosh(s) + s \sinh(s) - t \sinh(s)$.

Proof. For the first inequality, denote $A_1(s, t) := A(s, t) - \frac{(t-s)^2}{2}$. We prove that for any fixed $s \in \mathbb{R}$, $A_1(s, t) \geq 0$ for all $t \in \mathbb{R}$. If $s = 0$, we have $\cosh(t) - 1 \geq \frac{t^2}{2}$ for all $t \in \mathbb{R}$. If $s \neq 0$, the necessary condition for a minimum in t is $\frac{\partial A_1}{\partial t}(s, t) = 0$ which is equivalent to $\sinh(t) - \sinh(s) - t + s = 0$. The only solution of this equation is $t = s$ because the function $\sinh(t) - t$ is strictly monotonically increasing. It is left to observe that at $t = s$ we have $\frac{\partial^2 A_1}{\partial t^2} = \cosh(s) - 1 > 0$ and that $A_1(s, t = s) = 0$. For the second inequality, denote $A_2(s, t) := \frac{(\sinh(t) - \sinh(s))^2}{2} - A(s, t)$. If $t = 0$, the inequality $A_2(s, 0) \geq 0$ reduces to the inequality $q(s) := \frac{\sinh^2(s)}{2} - 1 + \cosh(s) - s \sinh(s) \geq 0$ which is true since the minimum of the function $q(s)$ is 0. If $t \neq 0$, the necessary condition for a minimum in s is $\frac{\partial A_2}{\partial s} = 0$ which is equivalent to $\cosh(s)(\sinh(s) - \sinh(t) - s + t) = 0$. The only solution of this equation is $s = t$. Now, it is left to observe that at $s = t$ we have $\frac{\partial^2 A_2}{\partial s^2} = \cosh(t)(\cosh(t) - 1) > 0$ and that $A_2(s = t, t) = 0$. \square

Since for the exact solution u we have $\rho_k(p^*) = \sinh(u + w)$ and $u = \operatorname{arsinh}(\rho_k(p^*)) - w$ a.e. in Ω_2 , we find that

$$\begin{aligned} D_F(v, -\Lambda^* p^*) &= \int_{\Omega_2} (k^2 \cosh(v + w) - lv + k^2 \sinh(u + w)u - k^2 \cosh(u + w) - \operatorname{div} p^* v) dx \\ &= \int_{\Omega_2} k^2 (\cosh(v + w) - \cosh(u + w) + u \sinh(u + w) - v \sinh(u + w)) dx. \end{aligned}$$

Similarly, $D_F(u, -\Lambda^* y^*) = \int_{\Omega_2} k^2 (\cosh(T) - \cosh(S) + S \sinh(S) - T \sinh(S)) dx$, where $T := \operatorname{arsinh}(\rho_k(p^*))$. The nonlinear quantities $D_F(v, -\Lambda^* p^*)$ and $D_F(u, -\Lambda^* y^*)$ measure the error in v and in $\operatorname{div} y^*$, respectively. Using inequality (3.22), we can represent these two measures in a form, which resembles the corresponding estimates in the case (2.12) of a quadratic functional F , namely,

$$\int_{\Omega_2} \frac{k^2}{2} (v - u)^2 dx \leq D_F(v, -\Lambda^* p^*) \leq \int_{\Omega_2} \frac{k^2}{2} (\sinh(v + w) - \sinh(u + w))^2 dx \quad (3.23)$$

and

$$\int_{\Omega_2} \frac{k^2}{2} (T - S)^2 dx \leq D_F(u, -\Lambda^* y^*) \leq \int_{\Omega_2} \frac{1}{2k^2} (\operatorname{div} p^* - \operatorname{div} y^*)^2 dx. \quad (3.24)$$

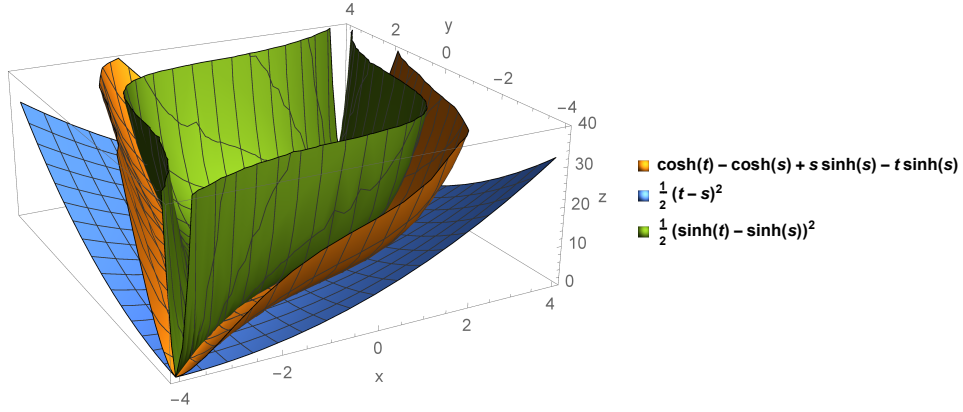


Figure 2: Constituting functions in the inequality (3.22).

Note that for $k \geq k_{\min} > 0$ in Ω the equivalences $\int_{\Omega} \frac{k^2}{2}(v-u)^2 dx \approx \|v-u\|_{L^2(\Omega)}^2$ and $\int_{\Omega} \frac{1}{2k^2}(\operatorname{div} p^* - \operatorname{div} y^*)^2 dx \approx \|\operatorname{div} y^* - \operatorname{div} p^*\|_{L^2(\Omega)}^2$ hold. Moreover, replacing the nonlinear term $k^2 \sinh(u+w)$ with u , the inequalities (3.23) and (3.24) reduce to the equalities for $D_F(v, -\Lambda^* p^*)$ and $D_F(u, -\Lambda^* y^*)$ in (2.12) because in this case the inverse function of $f(x) = x$ is again $f(x)$. The functions on the left-hand side, in the middle, and on the right-hand side in the inequality (3.2) are depicted on Figure 2. Further, if v is in a δ_1 -neighborhood of u in $L^\infty(\Omega)$ norm, then we can find a constant $C_1(\delta_1, \|u\|_{L^\infty(\Omega)}) > 1$ such that

$$\int_{\Omega_2} \frac{k^2}{2}(\sinh(v+w) - \sinh(u+w))^2 dx \leq C_1(\delta_1, \|u\|_{L^\infty(\Omega)}) \int_{\Omega_2} \frac{k^2}{2}(v-u)^2 dx. \quad (3.25)$$

Analogously, if $l \in L^\infty(\Omega_2)$ and $\|\operatorname{div}(y^* - p^*)\|_{L^\infty(\Omega)} \leq \delta_2$ (recall that when $l \in L^\infty(\Omega_2)$, $\operatorname{div} p^*$ is in $L^\infty(\Omega)$), then we can find a constant $C_2(\delta_2, \|\operatorname{div} p^*\|_{L^\infty(\Omega)}) < 1$ such that

$$C_2(\delta_2, \|\operatorname{div} p^*\|_{L^\infty(\Omega)}) \int_{\Omega_2} \frac{1}{2k^2}(\operatorname{div} p^* - \operatorname{div} y^*)^2 dx \leq \int_{\Omega_2} \frac{k^2}{2}(T-S)^2 dx. \quad (3.26)$$

Notice that if $k^2 \geq k_{\min} > 0$ in Ω , then everywhere in (3.23), (3.24), (3.25), and (3.26), the integrals are taken over the entire domain Ω . Now, the abstract error identity (2.11) takes the form

$$\begin{aligned} & \frac{1}{2} \|\nabla(u-v)\|^2 + \frac{1}{2} \|p^* - y^*\|_*^2 \\ & + \int_{\Omega_2} \frac{k^2}{2}(v-u)^2 dx + C_2(\delta_2, \|\operatorname{div} p^*\|_{L^\infty(\Omega)}) \int_{\Omega_2} \frac{1}{2k^2}(\operatorname{div} p^* - \operatorname{div} y^*)^2 dx \\ & \leq \frac{1}{2} \|\nabla(u-v)\|^2 + \frac{1}{2} \|p^* - y^*\|_*^2 + D_F(v, -\Lambda^* p^*) + D_F(u, -\Lambda^* y^*) = M_{\oplus}^2(v, y^*) \\ & \leq \frac{1}{2} \|\nabla(u-v)\|^2 + \frac{1}{2} \|p^* - y^*\|_*^2 \\ & + C_1(\delta_1, \|u\|_{L^\infty(\Omega)}) \int_{\Omega_2} \frac{k^2}{2}(v-u)^2 dx + \int_{\Omega_2} \frac{1}{2k^2}(\operatorname{div} y^* - \operatorname{div} p^*)^2 dx \end{aligned} \quad (3.27)$$

where we have used that $p^* = \epsilon \Lambda u = \epsilon \nabla u$. Relation (3.27) shows that the computable majorant $M_{\oplus}^2(v, y^*)$ is bounded from below and above by a multiple of one and the same error norm. Note that the left-hand side inequality in (3.27) is a stronger version of the left-hand inequality in (3.17). Since $D_F(v, -\Lambda^* p^*) \geq 0$ and $D_F(u, -\Lambda^* y^*) \geq 0$ we also obtain a guaranteed bound on the error in the combined energy norm:

$$\|\nabla(u - v)\|^2 + \|p^* - y^*\|_*^2 \leq 2M_{\oplus}^2(v, y^*). \quad (3.28)$$

From the pointwise equality

$$\begin{aligned} \frac{1}{\epsilon} |\epsilon \nabla v - y^*|^2 &= \frac{1}{\epsilon} |\epsilon \nabla(v - u) - (y^* - p^*)|^2 \\ &= \epsilon |\nabla(v - u)|^2 + \frac{1}{\epsilon} |y^* - p^*|^2 - 2(y^* - p^*) \cdot \nabla(v - u), \end{aligned} \quad (3.29)$$

after applying Young's inequality and integrating over Ω , we obtain a lower bound for the error in combined energy norm:

$$\frac{1}{2} \|\epsilon \nabla v - y^*\|_*^2 \leq \|\nabla(v - u)\|^2 + \|y^* - p^*\|_*^2 \quad (3.30)$$

Remark 3.2. *Integrating (3.29) over Ω we obtain the algebraic identity*

$$\|\epsilon \nabla v - y^*\|_*^2 = \|\nabla(v - u)\|^2 + \|y^* - p^*\|_*^2 - 2 \int_{\Omega} (y^* - p^*) \cdot \nabla(v - u) dx, \quad (3.31)$$

from which the Prager-Synge identity is derived. Comparing the last relation with (3.27), by using the fact that $M_{\oplus}^2(v, y^*)^2 = \frac{1}{2} \|\epsilon \nabla v - y^*\|_*^2 + D_F(v, -\Lambda^* y^*)$, we arrive at the relation

$$D_F(v, -\Lambda^* y^*) = D_F(v, -\Lambda^* p^*) + D_F(u, -\Lambda^* y^*) + \int_{\Omega} (y^* - p^*) \cdot \nabla(v - u) dx. \quad (3.32)$$

From here, it is seen that if the integral on the right-hand side is small compared to the other terms, then the error in v and $\text{div } y^*$ measured with $D_F(v, -\Lambda^* p^*) + D_F(u, -\Lambda^* y^*)$ is controlled mainly by the computable term $D_F(v, -\Lambda^* y^*)$ in the majorant $M_{\oplus}^2(v, y^*)$. Moreover, (3.31) enables us to give a practical estimation of the error in combined energy norm, which is very close to the real error in all of the experiments that we have conducted.

We end this section by presenting a near best approximation result. Contrary to the result in [18, Theorem 6.2], we do not make any restrictive assumptions on the meshes to ensure that the finite element approximations u_h are uniformly bounded in L^∞ norm. In our considerations, let V_h be a closed subspace of $H_0^1(\Omega)$ and let u_h be the unique minimizer of J over V_h , which is also the unique solution of the Galerkin problem

$$\begin{aligned} &\text{Find } u_h \in V_h \text{ such that} \\ &a(u_h, v) + \int_{\Omega} b(x, u_h + w) v dx = (l, v), \text{ for all } v \in V_h \cap L^\infty(\Omega). \end{aligned} \quad (3.33)$$

Then, using (2.9b) and the expression (3.20) for $D_G(\Lambda v, p^*)$, for any $v \in V_h$ we can write

$$\begin{aligned} &\|\nabla(u_h - u)\|^2 + 2D_F(u_h, -\Lambda^* p^*) = 2(J(u_h) - J(u)) \\ &\leq 2(J(v) - J(u)) = \|\nabla(v - u)\|^2 + 2D_F(v, -\Lambda^* p^*). \end{aligned}$$

Since $2D_F(u_h, -\Lambda^* p^*) \geq 0$, we obtain

$$\|\nabla(u_h - u)\|^2 \leq \inf_{v \in V_h} \left\{ \|\nabla(v - u)\|^2 + \int_{\Omega_2} k^2(\sinh(v + w) - \sinh(u + w))^2 dx \right\} \quad (3.34)$$

where we have used (3.23). Since we use the finite element method with P_1 Lagrange elements, let V_h be the corresponding space where h refers to the maximum element size. With $I_h(\varphi)$ we denote the Lagrange finite element interpolant of $\varphi \in C^0(\Omega)$. Using (3.34) we can show unqualified convergence of the finite element approximations u_h to u when $h \rightarrow 0$. Let $\varepsilon > 0$ and $\bar{u} \in C_0^\infty(\Omega)$ is such that $\|\nabla(\bar{u} - u)\|_{L^2(\Omega)} \leq \varepsilon$ and $\|\bar{u}\|_{L^\infty(\Omega)} \leq \|u\|_{L^\infty(\Omega)} + 2$. Also, let L be the Lipschitz constant in the inequality $|\sinh(s) - \sinh(t)| \leq L|s - t|$ for all $s, t \in [-2\|w\|_{L^\infty(\Omega_2)} - \bar{e} - 2, 2\|w\|_{L^\infty(\Omega_2)} + \bar{e} + 2]$. Then by applying the triangle inequality together with Young's inequality, we obtain

$$\begin{aligned} \|\nabla(u_h - u)\|^2 &\leq 2 \left(\|\nabla(I_h(\bar{u}) - \bar{u})\|^2 + \|\nabla(\bar{u} - u)\|^2 \right) \\ &+ 2 \left(\int_{\Omega} k^2(\sinh(I_h(\bar{u}) + w) - \sinh(\bar{u} + w))^2 dx + \int_{\Omega} k^2(\sinh(\bar{u} + w) - \sinh(u + w))^2 dx \right). \end{aligned} \quad (3.35)$$

For the first term in (3.35), by assuming mesh regularity, we have

$$\|\nabla(I_h(\bar{u}) - \bar{u})\|^2 + \|\nabla(\bar{u} - u)\|^2 \leq \epsilon_{\max} (C|\bar{u}|_2^2 h^2 + \varepsilon^2)$$

where $|\bar{u}|_2$ denotes the H^2 seminorm of \bar{u} and $C > 0$ is a constant depending on the mesh regularity. Using the fact that $\|I_h(\bar{u})\|_{L^\infty(\Omega)} \leq \|\bar{u}\|_{L^\infty(\Omega)} \leq \|u\|_{L^\infty(\Omega)} + 2$, for the second term in (3.35) we obtain the upper bound

$$\begin{aligned} &2k_{\max}^2 L^2 \left(\|I_h(\bar{u}) - \bar{u}\|_{L^2(\Omega)}^2 + \|\bar{u} - u\|_{L^2(\Omega)}^2 \right) \\ &\leq 2k_{\max}^2 L^2 C_F^2 \left(\|\nabla(I_h(\bar{u}) - \bar{u})\|_{L^2(\Omega)}^2 + \|\nabla(\bar{u} - u)\|_{L^2(\Omega)}^2 \right) \leq 2k_{\max}^2 L^2 C_F^2 (C|\bar{u}|_2^2 h^2 + \varepsilon^2). \end{aligned}$$

This shows that the right-hand side of (3.35) can be made as small as desired provided that we choose ε and h small enough and therefore $\|\nabla(u_h - u)\| \rightarrow 0$ when $h \rightarrow 0$. Moreover, (3.34) can be also used to obtain qualified convergence of u_h in energy norm under additional assumptions on the interface Γ , the meshes, and the regularity of u .

4 Numerical results

In the following we present numerical examples illustrating the functional a posteriori error equality (3.27) as well as the constituting terms of the equality. All numerical experiments are carried out in FreeFem++ developed and maintained by Frederich Hecht [14] and all pictures are generated in VisIt [4]. We solve adaptively the homogeneous nonlinear Problem (1.1) with $w := w_{h_{ref}} = g - z_{h_{ref}}$ where $z_{h_{ref}}$ is a good Galerkin finite element approximation of the solution z of

$$-\nabla \cdot (\epsilon \nabla z) = -k^2 \sinh(g) + l \quad \text{in } \Omega_1 \cup \Omega_2, \quad (4.1a)$$

$$[z]_\Gamma = 0, \quad (4.1b)$$

$$\left[\epsilon \frac{\partial z}{\partial n} \right]_\Gamma = 0, \quad (4.1c)$$

$$z = 0, \quad \text{on } \partial\Omega, \quad (4.1d)$$

for given functions g and l . We compare the accuracy of the adaptively computed solution u_h of (1.1) for $w = w_{h_{ref}}$ to the reference solution $z_{h_{ref}}$. The adaptive mesh refinement is based on the error indicator $\|\sqrt{2}\eta\|_{L^2(O_i)}$ where the function η is defined in (3.19) and η^2 is the integrand of the majorant $M_{\oplus}^2(v, y^*)$. The factor $\sqrt{2}$ accounts for the factor 2 in (3.28). More precisely, we find approximations u_h to the exact solution $u \in H_0^1(\Omega)$ of

$$\int_{\Omega} \epsilon \nabla u \cdot \nabla v dx + \int_{\Omega} b(x, u + w_{h_{ref}}) v dx = \int_{\Omega} l v dx = 0, \quad \forall v \in H_0^1(\Omega). \quad (4.2)$$

In all examples, we used piecewise constant parameters ϵ and k , and for $y^* \in H(\text{div}; \Omega)$, we used a patchwise equilibrated reconstruction of the numerical flux $\epsilon \nabla u_h$ based on [5]. More precisely, we find y^* in the Raviart-Thomas space RT_0 over the same mesh, such that its divergence is equal to the L^2 orthogonal projection of $k^2 \sinh(u_h + w) + l$ onto the space of piecewise constants.

Recall that

$$M_{\oplus}^2(v, y^*) = M_{\oplus}^2(v, p^*) + M_{\oplus}^2(u, y^*),$$

where $M_{\oplus}^2(v, y^*) = \frac{1}{2} \|\epsilon \nabla v - y^*\|_*^2 + D_F(v, -\Lambda^* y^*)$ and $M_{\oplus}^2(v, p^*) = J(v) - J(u) = \frac{1}{2} \|\nabla(v - u)\|^2 + D_F(v, -\Lambda^* p^*)$ is the primal error, whereas $M_{\oplus}^2(u, y^*) = I^*(p^*) - I^*(y^*) = \frac{1}{2} \|y^* - p^*\|_*^2 + D_F(u, -\Lambda^* y^*)$ is the dual error. Further, we use v for the approximate solution u_h and u for the reference solution $z_{h_{ref}}$ and define the efficiency index of the lower bound for the error in combined energy norm (3.30) by

$$I_{\text{Eff}}^{\text{CEN,Low}} := \frac{\frac{\sqrt{2}}{2} \|\epsilon \nabla v - y^*\|_*}{\sqrt{\|\nabla(v - u)\|^2 + \|y^* - p^*\|_*^2}}.$$

Similarly,

$$I_{\text{Eff}}^{\text{CEN,Up}} := \frac{\sqrt{2M_{\oplus}^2(v, y^*)}}{\sqrt{\|\nabla(v - u)\|^2 + \|y^* - p^*\|_*^2}}$$

defines the efficiency index of the upper bound (3.28) for the error in combined energy norm,

$$I_{\text{Eff}}^{\text{E}} := \frac{\sqrt{2M_{\oplus}^2(v, y^*)}}{\|\nabla(v - u)\|}$$

defines the efficiency index of the upper bound for the error in energy norm, and

$$P_{\text{rel}}^{\text{CEN}} := \frac{\|\epsilon \nabla v - y^*\|_*}{\sqrt{\|\nabla v\|^2 + \|y^*\|_*^2}}$$

defines the practical estimate of the relative error in combined energy norm.

4.1 Example 1 (2D)

In the first example, the domain Ω is a square with a side 20 with Ω_1 being a regular 15-sided polygon with a radius of its circumscribed circle equal to 2. The coefficients ϵ and k are

$$\epsilon(x) = \begin{cases} \epsilon_1 = 1, & x \in \Omega_1, \\ \epsilon_2 = 100, & x \in \Omega_2. \end{cases} \quad k(x) = \begin{cases} k_1 = 0.15, & x \in \Omega_1, \\ k_2 = 0.4, & x \in \Omega_2. \end{cases}$$

and

$$g = L \left(\exp \left(-b_1 \left(\frac{(x_1 - c_1)^2}{\sigma_1^2} - 1 \right) \right) - \exp \left(-b_2 \left(\frac{(x_2 - c_2)^2}{\sigma_2^2} - 1 \right) \right) \right),$$

$l = 0$, where $b_1 = 2 = b_2$, $c_1 = -1$, $c_2 = 6$, $\sigma_1 = \sigma_2 = 1.5$, $L = 0.8$. The reference solution $z_{h_{ref}}$ is computed on an adapted mesh with 50086142 triangles. Note that $k^2 = 0.0225$ in Ω_1 and $k^2 = 0.16$ in Ω_2 . The mesh adaptation is done with the built in function "adaptmesh" of freefem++. The localized error indicator $\|\sqrt{2}\eta\|_{L^2(O_i)}$, computed on each vertex patch O_i of the mesh, is compared to its average value over all patches and the local mesh size is divided by two if this average is smaller than the local value.

Table 1 illustrates the main error identity (2.10) and the convergence of its constituent parts. Further, it is seen that the dual error $2M_{\oplus}(u, y^*)$ dominates the primal error in this example. This is due to the fact that the term $2D_F(u, -\Lambda^*y^*)$, measuring the error in $\text{div } y^*$ (cf. (3.24) and (3.26)), is much larger than $\|\|\nabla(v - u)\|\|^2 + D_F(v, -\Lambda^*p^*)$, where $D_F(v, -\Lambda^*p^*)$ behaves like $\|v - u\|_{L^2(\Omega_2)}^2$ (cf. (3.23) and (3.25)). As we mentioned earlier, for y^* we use a partially equilibrated reconstruction of the numerical flux $\epsilon \nabla v$ which is the reason why the integral term in (3.31) is negligible compared to the combined energy norm of the error. This fact is confirmed by the values of the efficiency index of the lower bound (3.30).

Table 1: Example 1 (2D)

Example 1 (2D): $k_1 = 0.15$, $k_2 = 0.4$, $\epsilon_1 = 1$, $\epsilon_2 = 100$						
#elts	$\frac{\ v-u\ _0}{\ u\ _0}$ [%]	$\frac{\ \nabla(v-u)\ }{\ \nabla u\ }$ [%]	$\frac{\ y^*-p^*\ _*}{\ p^*\ _*}$ [%]	$2M_{\oplus}^2(v, y^*)$	$2M_{\oplus}^2(v, p^*)$	$2M_{\oplus}^2(u, y^*)$
196	15.0077	51.5582	86.1021	1778.14	66.5980	1711.54
347	5.69339	30.8534	41.7241	703.594	20.7780	682.816
630	4.20384	21.7715	31.4858	217.719	10.2201	207.498
1315	2.39552	15.8532	23.1244	76.8018	5.37574	71.4261
2865	1.87075	11.7353	17.1655	33.9310	2.94414	30.9869
5938	0.64611	7.93001	11.4692	16.0812	1.33874	14.7425
12006	0.36985	5.64786	8.23544	7.75232	0.67872	7.07360
24571	0.16023	3.94241	5.76054	3.85268	0.33039	3.52229
48483	0.08909	2.80265	4.09366	1.90043	0.16682	1.73361
97423	0.03961	1.97875	2.88455	0.96275	0.08304	0.87970
192905	0.02230	1.39832	2.03200	0.47524	0.04136	0.43388
386185	0.01015	0.99471	1.44616	0.24134	0.02082	0.22052

Table 2: Example 1 (2D)

Example 1 (2D): $k_1 = 0.15$, $k_2 = 0.4$, $\epsilon_1 = 1$, $\epsilon_2 = 100$				
#elts	$\ \ \nabla(v - u)\ \ ^2$	$\ y^* - p^*\ _*^2$	$2D_F(v, -\Lambda^*p^*)$	$2D_F(u, -\Lambda^*y^*)$
196	56.5057	157.588	10.0923	1553.95
347	20.2350	37.0058	0.54296	645.811
630	10.0756	21.0729	0.14450	186.425
1315	5.34235	11.3668	0.03338	60.0593
2865	2.92742	6.26338	0.01671	24.7235
5938	1.33673	2.79619	0.00200	11.9462
12006	0.67805	1.44169	0.00067	5.63191
24571	0.33038	0.70538	0.00001	2.81691
48483	0.16696	0.35622	0.00000	1.37739
97423	0.08323	0.17687	0.00000	0.70283
192905	0.04156	0.08777	0.00000	0.34611
386185	0.02103	0.04445	0.00000	0.17606

Table 3: Example 1 (2D)

Example 1 (2D): $k_1 = 0.15$, $k_2 = 0.4$, $\epsilon_1 = 1$, $\epsilon_2 = 100$						
#elts	$\frac{D_F(v, -\Lambda^* y^*)}{M_{\oplus}^2(v, y^*)} [\%]$	$I_{\text{Eff}}^{\text{CEN,Low}}$	$I_{\text{Eff}}^{\text{CEN,Up}}$	$I_{\text{Eff}}^{\text{E,Up}}$	$P_{\text{rel}}^{\text{CEN}} [\%]$	True rel. error in CEN [%]
196	89.0701	0.67371	2.88191	5.60966	74.6973	70.9641
347	92.4942	0.67919	3.50597	5.89671	36.2638	36.6935
630	85.9525	0.70066	2.64380	4.64848	27.1574	27.0680
1315	78.2616	0.70681	2.14392	3.79158	19.9383	19.8250
2865	72.8992	0.70729	1.92142	3.40452	14.7523	14.7032
5938	74.3009	0.70708	1.97256	3.46846	9.87419	9.85973
12006	72.6473	0.70722	1.91238	3.38130	7.06762	7.06119
24571	73.1176	0.70708	1.92864	3.41485	4.93753	4.93591
48483	72.4826	0.70694	1.90588	3.37371	3.50789	3.50805
97423	73.0084	0.70678	1.92392	3.40108	2.47256	2.47347
192905	72.8486	0.70629	1.91692	3.38145	1.74226	1.74418
386185	72.9912	0.70546	1.91972	3.38748	1.23829	1.24114

In Table 3 we can see that $I_{\text{Eff}}^{\text{CEN,Low}}$ is approximately equal to $0.7071 \approx \frac{\sqrt{2}}{2}$. The value of the efficiency index with respect to the combined energy norm and the value of the ratio $D_F(v, -\Lambda^* y^*)/M_{\oplus}^2(v, y^*)$ are also coupled in the sense that if we have only one of these two quantities, we can estimate the other one by using the main error equality (3.27). This estimation is accurate because the integral term in (3.32) is very close to zero and therefore $D_F(v, -\Lambda^* y^*) \approx D_F(v - \Lambda^* p^*) + D_F(u - \Lambda^* y^*)$. One more consequence of using a partially equilibrated flux is that we obtain a very accurate practical estimate of the absolute and relative error in combined energy norm as illustrated in the last two columns of Table 3.

Figure 5 depicts a mesh that is a part of a sequence of meshes obtained by mesh adaptation using the localized functional error indicator $\|\sqrt{2}\eta\|_{L^2(O_i)}$. Figure 6 depicts a mesh with approximately the same number of elements but obtained by mesh adaptation using the error indicator $\|\epsilon \nabla v - y^*\|_{*(O_i)}$. The mesh in Figure 5 is refined mainly where the error in $\text{div } y^*$ is the dominant part of the error $M_{\oplus}^2(v, -\Lambda^* p^*) + M_{\oplus}^2(u, -\Lambda^* y^*)$. On the other hand, the mesh in Figure 6 is refined most around the extrema of the solution. Figure 8 depicts the minimal set of elements K of a mesh T_h that contains at least 30% of the total indicated error $\sum_{K \in T_h} \|\epsilon \nabla v - y^*\|_{*(K)}$ (greedy algorithm with a bulk factor of 0.3), where T_h is part of the same sequence as the mesh illustrated in Figure 6.

Figure 10 depicts the elements marked by the greedy algorithm using a bulk factor of 0.5 and employing the true error $\sqrt{2M_{\oplus}^2(v, p^*) + 2M_{\oplus}^2(u, y^*)}$ as indicator. Figure 9 depicts elements which are marked additionally or fail to be marked by the same greedy algorithm when employing the functional error indicator $\|\sqrt{2}\eta\|_{L^2(O_i)}$ for the same bulk factor. The ratio of the number of these differently marked elements, that is, elements which are marked by one of the two methods but not by the other one, and the total number of elements is 0.022 and the ratio of the number of differently marked elements to the number of marked elements using the true error is 0.048 (see Table 4). Comparing the indicated error and the true error elementwise, one finds that the error indicator generated by the majorant $M_{\oplus}^2(v, y^*)$ reproduces the local distribution of the error with a very high accuracy. This is also confirmed by Figure 4 where it can be seen that all error measures are almost identical in both cases of adaptive mesh refinement. Mesh adaptation based on the functional error indicator $\|\sqrt{2}\eta\|_{L^2(O_i)}$ instead of the error indicator $\|\epsilon \nabla v - y^*\|_{*(O_i)}$ (see Figure 3) yields approximately twice smaller efficiency indexes in energy and combined energy norms and approximately twice smaller values for the full error $M_{\oplus}^2(v, p^*) + M_{\oplus}^2(u, y^*)$ on meshes

with a comparable number of elements. The reason for the higher efficiency indexes is that no adaptive control is applied on the nonlinear part of the error measure in (3.27), and consequently, the ratio $D_F(v, -\Lambda^*y^*)/M_{\oplus}^2(v, y^*)$ is increasing, reaching values close to 100% on fine meshes. However, the error in $\|\|\nabla(v - u)\|\|$ and $\|\|y^* - p^*\|\|_*$ might be a little higher in the case of the functional error indicator $\|\sqrt{2}\eta\|_{L^2(O_i)}$. For example, on the mesh from Figure 8 with 24 122 elements, $M_{\oplus}^2(v, p^*) + M_{\oplus}^2(u, y^*) = 3.8314$, $\|\|\nabla(v - u)\|\| = 0.4674$, $\|\|y^* - p^*\|\|_* = 0.6540$, whereas on a mesh with 24 571 elements from the sequence adapted with the indicator $\|\sqrt{2}\eta\|_{L^2(O_i)}$, we obtained a value of 1.9263 for $M_{\oplus}^2(v, y^*)$, and 0.574791 and 0.8399 for $\|\|\nabla(v - u)\|\|$ and $\|\|y^* - p^*\|\|_*$, respectively. This shows that by reducing the error in $\text{div } y^*$ the functional error indicator $\|\sqrt{2}\eta\|_{L^2(O_i)}$ provides a better approximation for the primal and dual problem together.

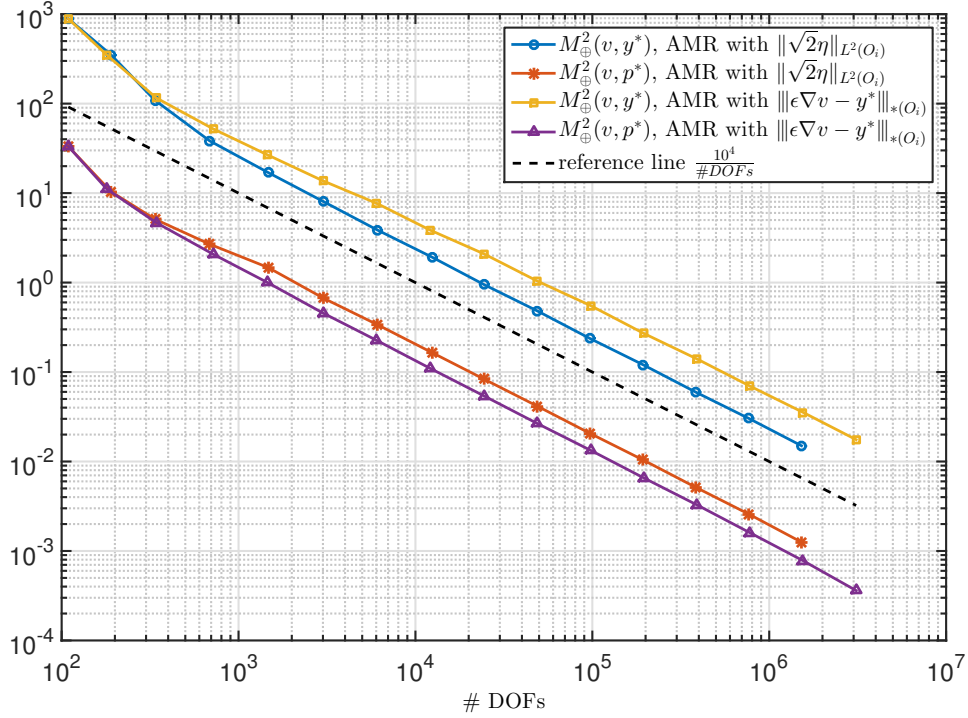


Figure 3: Comparison of errors for AMR based on the functional error indicator $\|\sqrt{2}\eta\|_{L^2(O_i)}$ versus AMR based on the indicator $\|\|\epsilon \nabla v - y^*\|\|_{*(O_i)}$.

Table 4: Example 1 (2D)

Example 1 (2D): $k_1 = 0.15$, $k_2 = 0.4$, $\epsilon_1 = 1$, $\epsilon_2 = 100$			
#elts	#marked elts with true error	#differently marked elts	differently marked elts in % of all mesh elts
196	62	6	3.06122
347	150	10	2.88184
630	288	14	2.22222
1315	632	39	2.96578
2865	1439	113	3.94415
5938	2949	216	3.63759
12006	5981	534	4.44778
24571	12099	961	3.91111
48483	24194	2233	4.60574
97423	47784	4012	4.11812

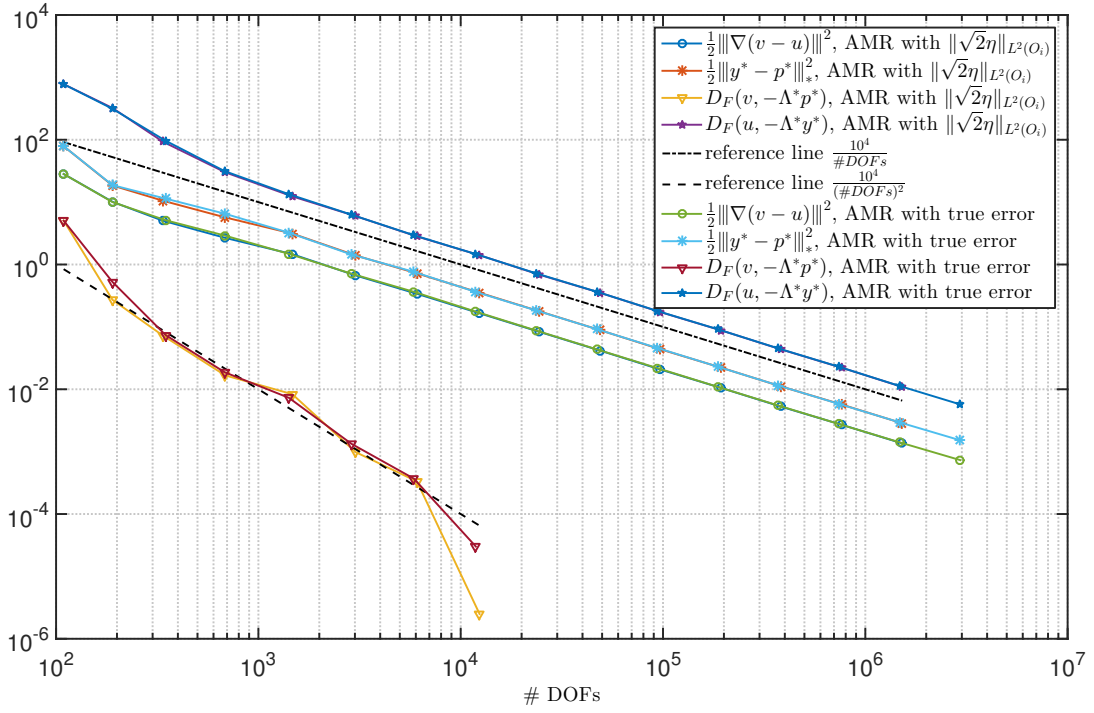


Figure 4: Comparison of errors for AMR based on the functional error indicator $\|\sqrt{2}\eta\|_{L^2(O_i)}$ versus AMR based on the indicator generated by the true error $\sqrt{2M_{\oplus}^2(v, p^*) + 2M_{\oplus}^2(u, y^*)}$.

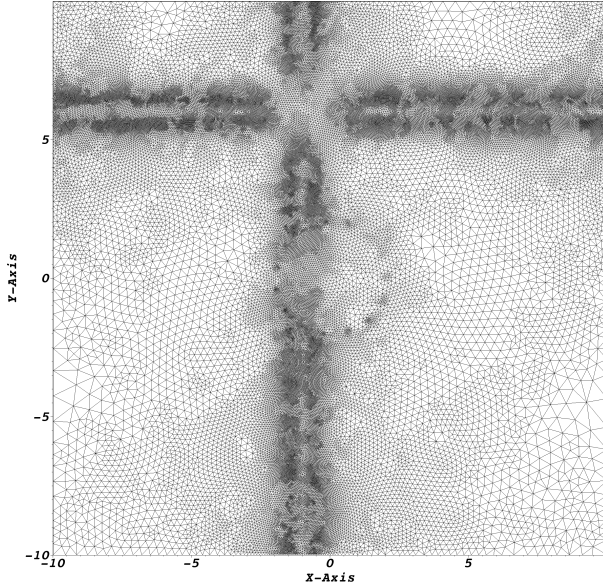


Figure 5: Mesh on the 9th level of AMR (97 423 elements) based on the error indicator $\|\sqrt{2}\eta\|_{L^2(O_i)}$ with flux equilibration for y^* .

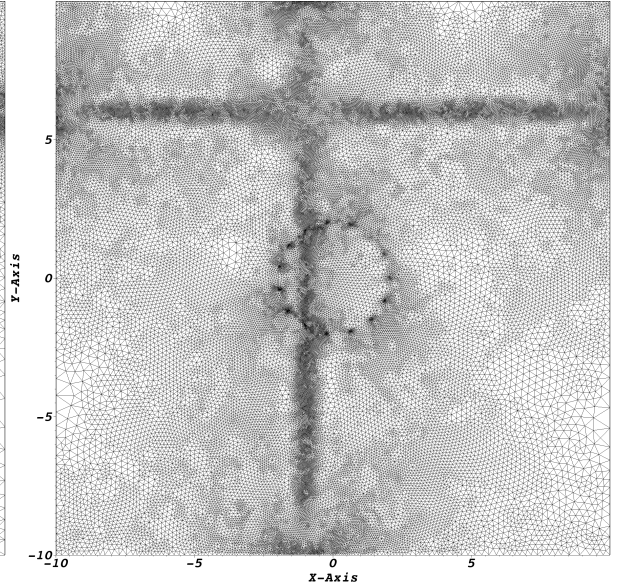


Figure 6: Mesh on level 9th level of AMR (97 353 elements) based on the error indicator $\|\epsilon\nabla v - y^*\|_{*(O_i)}$ with flux equilibration for y^* .

In the following we want to demonstrate that flux equilibration is indeed an important subtask to make the proposed error bounds reliable and efficient. For this purpose, we use a simple global gradient averaging procedure, i.e. project the numerical flux $\epsilon\nabla v \in L^2(\Omega)$ onto the subspace $[V_h]^2$, where V_h is the finite element space of continuous piecewise linear functions. We then solve adaptively Example 1 once by applying the functional error indicator $\|\sqrt{2}\eta\|_{L^2(O_i)}$ and once by applying the error indicator $\|\epsilon\nabla v - y^*\|_{*(O_i)}$. Figure 11 shows an adapted mesh with 563 965 elements which is a part of a sequence of meshes

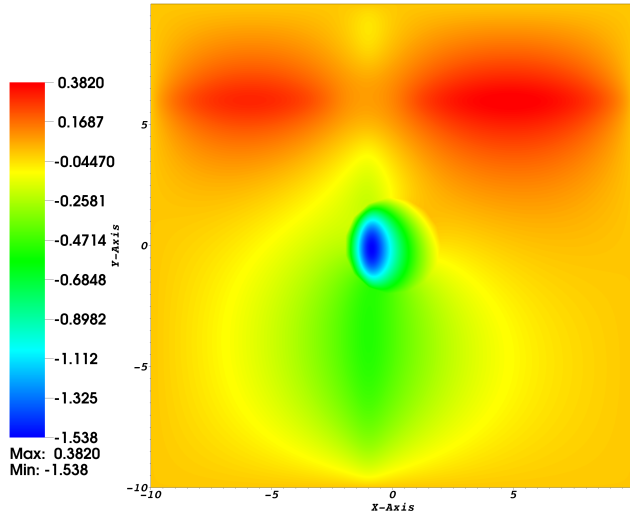


Figure 7: Reference solution for Example 1 (2D).

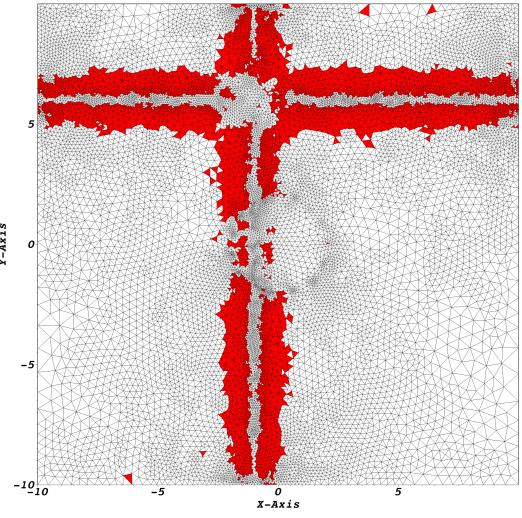


Figure 8: Mesh on the 7th level of AMR (24122 elements) based on the error indicator $\|\epsilon \nabla v - y^*\|_{*(O_i)}$ with flux equilibration for y^* . Marked elements using the error indicator $\|\sqrt{2}\eta\|_{L^2(K)}$ applying greedy algorithm with bulk factor 0.3.

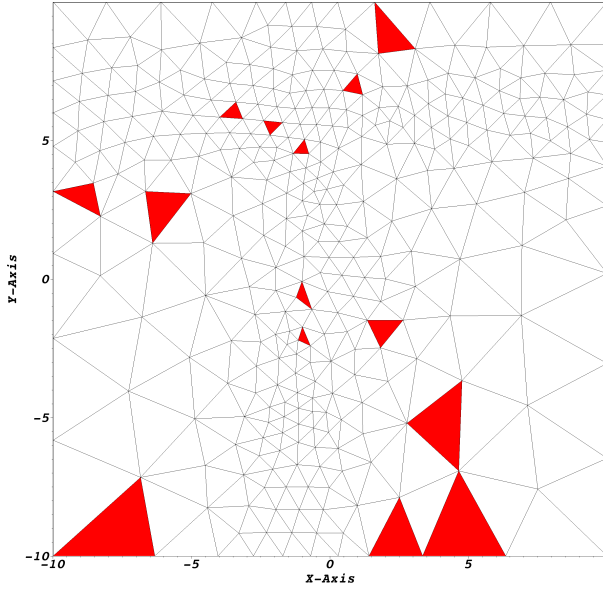


Figure 9: Mesh on the 2nd level of AMR (630 elements) based on the error indicator $\|\sqrt{2}\eta\|_{L^2(O_i)}$ with flux equilibration for y^* . Differently marked elements using the error indicator $\|\sqrt{2}\eta\|_{L^2(K)}$ as compared to the elements marked when using the true error $M_{\oplus}^2(v, -\Lambda^* p^*) + M_{\oplus}^2(u, -\Lambda^* y^*)$ applying greedy algorithm with bulk factor 0.5.

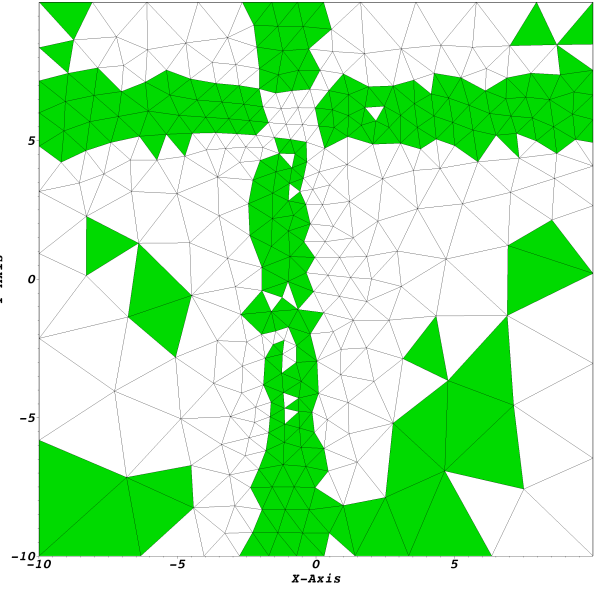


Figure 10: Mesh on the 2nd level of AMR (630 elements) based on the error indicator $\|\sqrt{2}\eta\|_{L^2(O_i)}$ with flux equilibration for y^* . Marked elements using the true error $\sqrt{2M_{\oplus}^2(v, p^*) + 2M_{\oplus}^2(u, y^*)}$ applying greedy algorithm with bulk factor 0.5.

obtained by applying the functional error indicator with gradient averaging for y^* while Figure 12 shows a mesh with 444092 elements which is part of a sequence of meshes adapted using the second indicator with gradient averaging for y^* . It can be seen by comparing with the results based on flux equilibration for y^* that the mesh in Ω_2 close to the interface Γ is refined too much for both error indicators. Apart from that, the

meshes on Figures 12 and 6 look quite similar, unlike the meshes on Figures 11 and 5. For meshes with similar number of elements, by applying the indicator $\|\|\epsilon \nabla v - y^*\|_{*(O_i)}$ using flux equilibration versus gradient averaging we obtained around 30% larger values for the error $\|\|\nabla(v - u)\|$ and 60% larger values for the error $\|\|y^* - p^*\|_*$. The difference in the errors when applying the functional indicator $\|\sqrt{2}\eta\|_{L^2(O_i)}$ with flux equilibration versus with gradient averaging for y^* is even more drastic—between 40% and 180% larger error $\|\|\nabla(v - u)\|$ and between 64% and 66% larger error $\|\|y^* - p^*\|_*$ for meshes with between 21 528 and 563 965 elements. In both cases we obtained an increasing sequence of efficiency indexes with respect to energy and combined energy norms reaching values of 133 and 107 with the functional error indicator on a mesh with 2 089 022 elements, and 570 and 269 with the error indicator $\|\|\epsilon \nabla v - y^*\|_{*(O_i)}$ on a mesh with 2 954 218 elements. This is due to the fact that the nonlinear term $D_F(u, -\Lambda^* y^*)$, which measures the error in $\text{div } y^*$ (see (3.24) and (3.26)), dominates the other terms in the nonlinear measure $M_{\oplus}^2(v, p^*) + M_{\oplus}^2(u, y^*)$ for the error, reaching more than 99.99% of it in both cases. In both experiments with gradient averaging for y^* , increasing values of $D_F(u, -\Lambda^* y^*)$ are in correspondence with increasing error $\|\|\text{div } y^* - \text{div } p^*\|_{L^2(\Omega)}$ and increasing efficiency indexes.

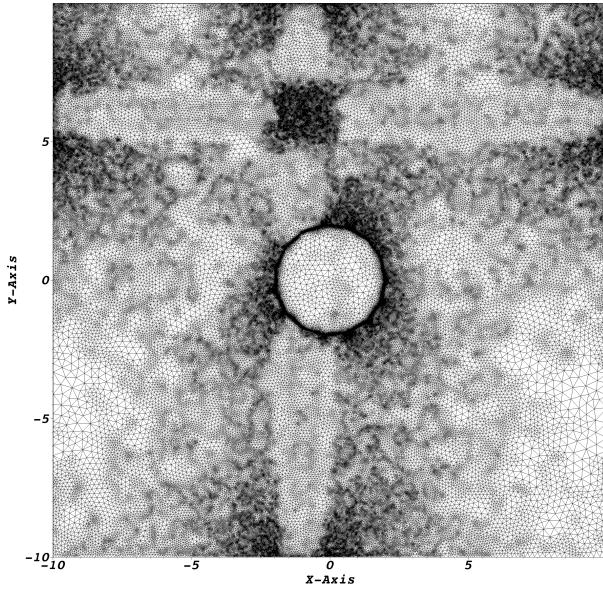


Figure 11: Mesh with 563 965 elements, adapted using the error indicator $\|\sqrt{2}\eta\|_{L^2(O_i)}$ with gradient averaging for y^* .

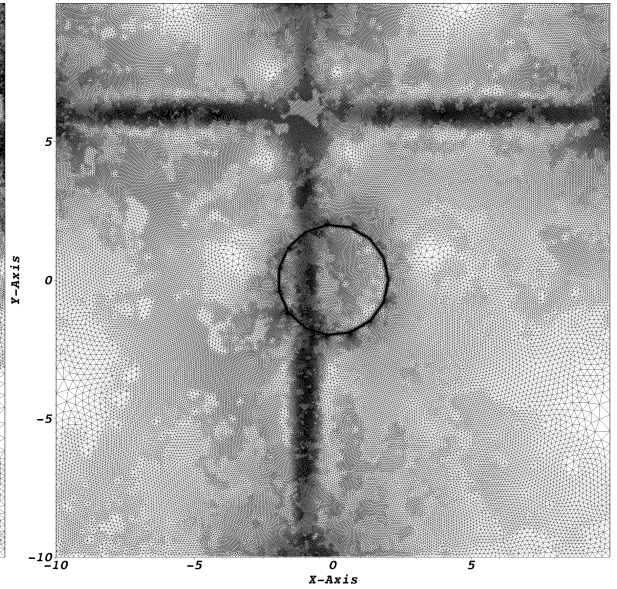


Figure 12: Mesh with 444 092 elements, adapted using the error indicator $\|\|\epsilon \nabla v - y^*\|_{*(O_i)}$ with gradient averaging for y^* .

4.2 Example 2 (2D)

Figures 14 and 16 show the dependence of the meshes on the indicator for another example. Here, $\epsilon_1 = 1$, $\epsilon_2 = 100$, $k_1 = 0.2$, $k_2 = 0.3$. The function $g = \exp\left(-b_1\left(\frac{|x-c_1|^2}{\sigma_1^2} - 1\right)\right) - \exp\left(-b_2\left(\frac{|x-c_2|^2}{\sigma_2^2} - 1\right)\right)$ and $l = \exp\left(-b_3\left(\frac{|x|^2}{\sigma_3^2} - 1\right)\right) \sin\left(\frac{x_1 x_2}{4}\right)$, where $b_1 = 2.2$, $b_2 = 2.5$, $b_3 = 6$, $c_1 = (-1, 0)$, $c_2 = (5, 5)$, $\sigma_1 = \sigma_2 = 2$, $\sigma_3 = 10$. The indicator $\|\|\epsilon \nabla v - y^*\|_{*(O_i)}$ approximates well the elementwise error in combined energy norm but does not capture the rest of the error which is a result from the nonlinearity $k^2 \sinh(u + w)$ and the right-hand side l in (1.1). On the other hand, the term $D_F(v, -\Lambda^* y^*)$ controls the error $D_F(v, -\Lambda^* p^*) + D_F(u, -\Lambda^* y^*)$ and this is the reason why the mesh on Figure 14 resembles the wavy features of the function $f = -k^2 \sinh(u + w) + l$.

The isolines of the reference solution and of the function f are depicted on Figures 15 and 13.

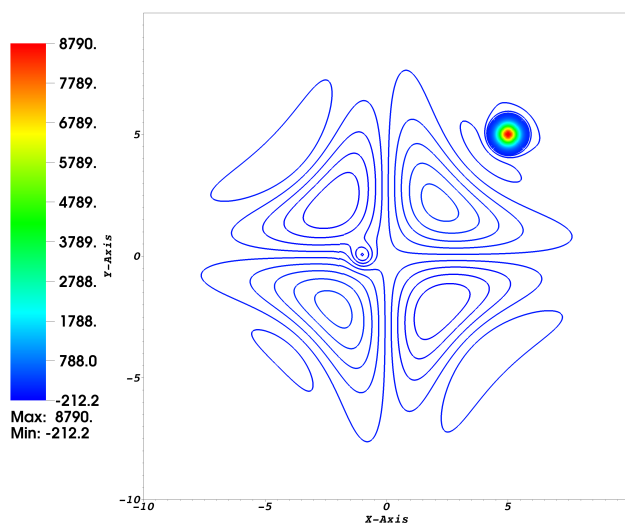


Figure 13: Function $f = -k^2 \sinh(u + w) + l$.

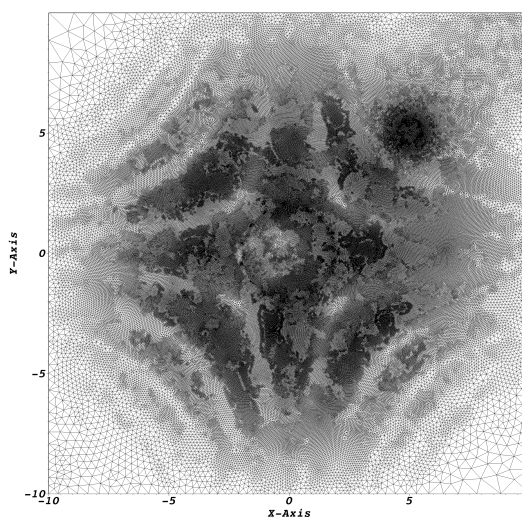


Figure 14: Mesh with 395 935 elements, obtained by AMR using the error indicator $\|\sqrt{2}\eta\|_{L^2(O_i)}$ with flux equilibration for y^* .

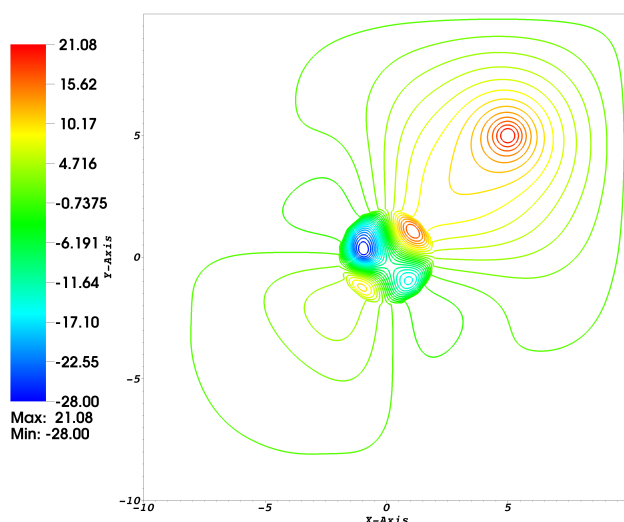


Figure 15: Reference solution.

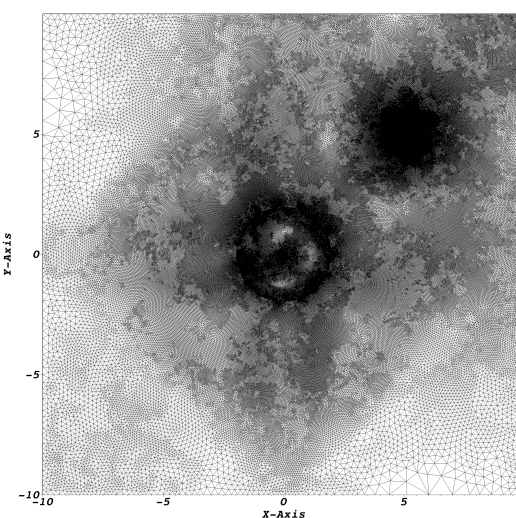


Figure 16: Mesh with 555 489 elements, obtained by AMR using the error indicator $\|\epsilon \nabla v - y^*\|_{*(O_i)}$ with flux equilibration for y^* .

4.3 Example 3 (3D)

In the third example, the computational domain Ω is a cube of side length 20 Angstroms with a triangulated water molecule Ω_1 in it. The diameter of the water molecule, which is positioned in the center of the cube, is about 2.75 Angstroms. Its shape is not changed during the mesh adaptation process. The surface mesh of the water molecule is taken from [1]. Figure 17 illustrates the initial tetrahedral mesh, which consists of 60 222 elements. It is generated using TetGen [27] and adaptively refined with the help of mmg3d [7]. Using the localized error indicator $\|\sqrt{2}\eta\|_{L^2(O_i)}$ computed on each vertex patch O_i of the mesh,

a new local mesh size at each vertex is defined by the formula

$$h_i^{\text{new}} = h_i^{\text{old}} \left(\max \left\{ \min \left\{ \frac{\text{AM} \{ \|\sqrt{2}\eta\|_{L^2(O_j)} \}}{\|\sqrt{2}\eta\|_{L^2(O_i)}}, 1 \right\}, 0.35 \right\} \right)$$

and supplied to mmg3d, where $\text{AM} \{ \|\sqrt{2}\eta\|_{L^2(O_j)} \}$ is the arithmetic mean of $\{ \|\sqrt{2}\eta\|_{L^2(O_j)} \}$ over all vertex patches O_j . The coefficients ϵ and k for this example are typical for electrostatic computations in biophysics using the PBE and are given by

$$\epsilon(x) = \begin{cases} \epsilon_1 = 2, & x \in \Omega_1, \\ \epsilon_2 = 80, & x \in \Omega_2. \end{cases} \quad k(x) = \begin{cases} k_1 = 0, & x \in \Omega_1, \\ k_2 = 0.84, & x \in \Omega_2. \end{cases}$$

Moreover, we assume that the problem is homogeneous, i.e., $l = 0$, and

$$g = \exp \left(-b_1 \left(\frac{|x - c_1|^2}{\sigma_1^2} - 1 \right) \right) - \exp \left(-b_2 \left(\frac{|x - c_2|^2}{\sigma_2^2} - 1 \right) \right) \\ + \exp \left(-b_3 \left(\frac{|x - c_3|^2}{\sigma_3^2} - 1 \right) \right) + \exp \left(-b_4 \left(\frac{|x - c_4|^2}{\sigma_4^2} - 1 \right) \right),$$

where $b_1 = b_2 = b_3 = b_4 = 2.3$, $c_1 = (1, 1, 0)$, $c_2 = (4, 4, 0)$, $c_3 = (0, 6, 0)$, $c_4 = (-5, 0, 0)$, $\sigma_1 = \sigma_2 = \sigma_3 = \sigma_4 = 2$. The reference solution $z_{h_{ref}}$ is computed on an adapted mesh with 79 917 007 tetrahedrons.

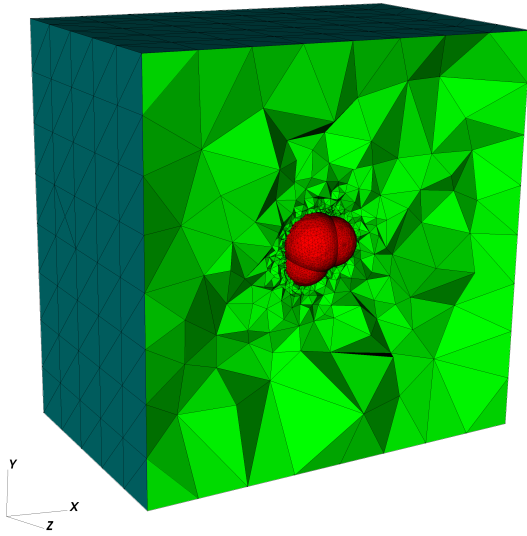


Figure 17: Initial mesh in Example 3 consisting of 60 222 tetrahedrons.

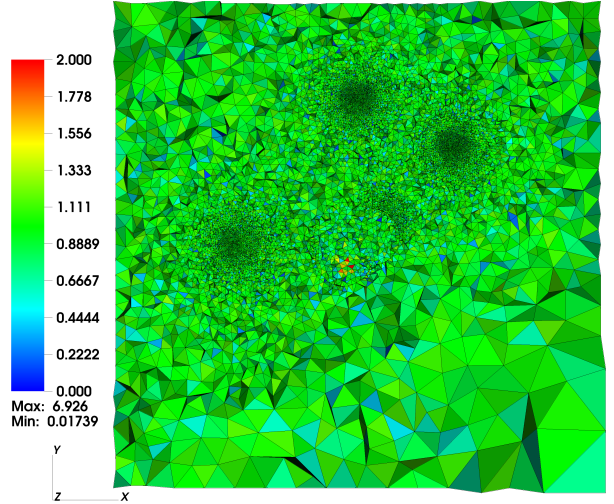


Figure 18: Ratio of error indicator $\|\epsilon \nabla v - y^*\|_*$ and combined energy norm of the error, elementwise. Mesh on the 4th level of AMR ($1.1736e+06$ elements) in Example 3 using the error indicator $\|\sqrt{2}\eta\|_{L^2(O_i)}$ with flux equilibration for y^* .

Since $l = 0$ in Ω_1 is a constant function, the patchwise reconstruction from [5] produces a flux y^* with zero divergence in Ω_1 and therefore the reliability of our majorant is guaranteed. In this example we achieve a very tight guaranteed bound on the error in combined energy norm, as well as in energy norm. The efficiency index $I_{\text{Eff}}^{\text{CEN}, \text{UP}}$ settles at around 1.05 and the efficiency index $I_{\text{Eff}}^{\text{E}, \text{UP}}$ decreases to 1.30 (see Table 6). This is in a good agreement with the fact that in this example the ratio $D_F(v, -\Lambda^* y^*) / M_{\oplus}^2(v, y^*)$ is well controlled and decreases to around 10% (see column 2 in Table 7). We also note that in this example we obtained very similar results with the error indicator $\|\epsilon \nabla v - y^*\|_{*(O_i)}$.

For the efficiency index $I_{\text{Eff}}^{\text{CEN,Low}}$ of the lower bound on the combined energy norm of the error we obtain values converging to approximately 0.7071 which is the approximate value of $\frac{\sqrt{2}}{2}$ (see column 3 in Table 6). This means that the combined energy norm of the error $\sqrt{\|\nabla(v-u)\|^2 + \|y^* - p^*\|_*^2}$ is practically equal to $\|\epsilon \nabla v - y^*\|_*$.

Another consequence of this fact is the good accuracy of the practical estimation $P_{\text{rel}}^{\text{CEN}}$ of the relative error in combined energy norm (see columns 6 and 7 in Table 6). The tight bounds on the error also enable us to compute tight and guaranteed upper bounds on the relative error in energy norm and combined energy norm as follows:

$$\frac{\|\nabla(v-u)\|}{\|\nabla u\|} \leq \frac{\sqrt{2M_{\oplus}^2(v, y^*)}}{\|\nabla v\| - \sqrt{2M_{\oplus}^2(v, y^*)}} =: \text{RE}^{\text{Up}} \quad (4.3a)$$

$$\frac{\sqrt{\|\nabla(v-u)\|^2 + \|y^* - p^*\|_*^2}}{\sqrt{\|\nabla v\|^2 + \|y^*\|_*^2}} \leq \frac{\sqrt{2M_{\oplus}^2(v, y^*)}}{\sqrt{\|\nabla v\|^2 + \|y^*\|_*^2} - \sqrt{2M_{\oplus}^2(v, y^*)}} =: \text{RCEN}^{\text{Up}} \quad (4.3b)$$

where (4.3a) is valid if $\|\nabla v\| - \sqrt{2M_{\oplus}^2(v, y^*)} > 0$ and (4.3b) is valid if $\sqrt{\|\nabla v\|^2 + \|y^*\|_*^2} - \sqrt{2M_{\oplus}^2(v, y^*)} > 0$.

Similarly, we compute a tight and guaranteed lower bound for the relative error in combined energy norm by

$$\text{RCEN}^{\text{Low}} := \frac{\frac{1}{\sqrt{2}} \|\epsilon \nabla v - y^*\|_*}{\sqrt{\|\nabla v\|^2 + \|y^*\|_*^2} + \sqrt{2M_{\oplus}^2(v, y^*)}} \leq \frac{\sqrt{\|\nabla(v-u)\|^2 + \|y^* - p^*\|_*^2}}{\sqrt{\|\nabla v\|^2 + \|y^*\|_*^2}}. \quad (4.4)$$

Table 5: Example 3 (3D)

Example 3 (3D): $k_1 = 0, k_2 = 0.84, \epsilon_1 = 2, \epsilon_2 = 80$						
#elts	$\frac{\ v-u\ _0}{\ u\ _0}$ [%]	$\frac{\ \nabla(v-u)\ }{\ \nabla u\ }$ [%]	$\frac{\ y^* - p^*\ _*}{\ p^*\ _*}$ [%]	$2M_{\oplus}^2(v, y^*)$	$2M_{\oplus}^2(v, p^*)$	$2M_{\oplus}^2(u, y^*)$
60222	76.8320	108.015	167.589	425569	117373	308196
103236	11.9257	46.3306	55.1210	47104.5	17845.0	29259.5
222118	1.09233	17.7353	14.9578	4484.44	2224.69	2259.75
552936	0.49820	8.67222	7.09062	965.067	513.706	451.361
1.1736e+06	0.25609	6.58075	5.33661	539.734	295.254	244.481
2.05668e+06	0.17094	5.37625	4.18207	350.648	197.016	153.631
2.97315e+06	0.12317	4.73466	3.53852	265.167	152.783	112.385
3.90692e+06	0.10071	4.32886	3.12966	216.336	127.703	88.6336

Table 6: Example 3 (3D)

Example 3 (3D): $k_1 = 0, k_2 = 0.84, \epsilon_1 = 2, \epsilon_2 = 80$				
#elts	$\ \nabla(v-u)\ ^2$	$\ y^* - p^*\ _*^2$	$2D_F(v, -\Lambda^* p^*)$	$2D_F(u, -\Lambda^* y^*)$
60222	79487.0	191346	37886.0	116850
103236	14623.9	20699.7	3221.12	8559.78
222118	2142.92	1524.28	81.7757	735.474
552936	512.376	342.528	1.32980	108.833
1.1736e+06	295.039	194.026	0.21458	50.455
2.05668e+06	196.919	119.155	0.09743	34.4762
2.97315e+06	152.724	85.3044	0.05857	27.0805
3.90692e+06	127.666	66.7303	0.03663	21.9033

In Table 8 we show the computed by (4.3) and (4.4) guaranteed bounds on the relative errors.

Table 7: Example 3 (3D)

Example 3 (3D): $k_1 = 0, k_2 = 0.84, \epsilon_1 = 2, \epsilon_2 = 80$						
#elts	$\frac{D_F(v, -\Lambda^* y^*)}{M_{\oplus}^2(v, y^*)} [\%]$	$I_{\text{Eff}}^{\text{CEN,Low}}$	$I_{\text{Eff}}^{\text{CEN,Up}}$	$I_{\text{Eff}}^{\text{E,Up}}$	$P_{\text{rel}}^{\text{CEN}} [\%]$	True rel. error in CEN [%]
60222	40.0541	0.68627	1.25353	2.31386	92.8434	140.985
103236	20.4500	0.72828	1.15478	1.79473	47.6870	50.9159
222118	16.1172	0.71615	1.10583	1.44661	16.4040	16.4054
552936	11.2249	0.70786	1.06248	1.37241	7.90966	7.92099
1.1736e+06	9.33477	0.70731	1.05053	1.35254	5.98505	5.99106
2.05668e+06	9.82289	0.70725	1.05327	1.33442	4.81343	4.81632
2.97315e+06	10.2057	0.70722	1.05547	1.31767	4.17784	4.17960
3.90692e+06	10.1194	0.70719	1.05492	1.30175	3.77592	3.77716

Table 8: Example 3 (3D)

Example 3 (3D): $k_1 = 0, k_2 = 0.84, \epsilon_1 = 2, \epsilon_2 = 80$			
#elts	RCEN ^{Low} [%]	RCEN ^{Up} [%]	RE ^{Up} [%]
60222	26.8329	2480.32	-
103236	20.9158	98.4934	310.049
222118	9.76945	21.6027	33.9219
552936	5.14869	9.14078	13.4714
1.1736e+06	3.97619	6.69650	9.75647
2.05668e+06	3.23651	5.33417	7.72193
2.97315e+06	2.82755	4.60886	6.64970
3.90692e+06	2.56630	4.14555	5.96873

As a remark, we note that the efficiency indexes with respect to the energy and combined energy norms of the error can be improved if we use a flux reconstruction in a bigger space, say RT_1 , which has better approximation properties. In this way the error in $\text{div } y^*$ will decrease and as a result, the term $D_F(v, -\Lambda^* y^*)$ and consequently the dual part of the error $2M_{\oplus}^2(u, y^*) = \| \| y^* - p^* \| \|_*^2 + D_F(u, -\Lambda^* y^*)$ will constitute a smaller part of the whole majorant and the error, respectively. Even better, we can minimize the majorant with respect to y^* in a subspace of $H(\text{div}; \Omega)$ like RT_0 , possibly on another finer mesh. Note that in the limit case we have $\inf_{y^* \in H(\text{div}; \Omega)} M_{\oplus}^2(v, y^*) = M_{\oplus}^2(v, p^*) = \frac{1}{2} \| \| \nabla(v - u) \| \| ^2 + D_F(v, -\Lambda^* p^*)$ and the dual error completely vanishes. In this case,

$$I_{\text{Eff}}^{\text{CEN,Up}} = I_{\text{Eff}}^{\text{E}} = \frac{\sqrt{2M_{\oplus}^2(v, p^*)}}{\| \| \nabla(v - u) \| \|} = \frac{\sqrt{\| \| \nabla(v - u) \| \| ^2 + 2D_F(v, -\Lambda^* p^*)}}{\| \| \nabla(v - u) \| \|}$$

where the last ratio tends to 1 because by (3.25) the term $D_F(v, -\Lambda^* p^*) \sim \| \| v - u \| \|_{L^2(\Omega)}^2$ and has a higher order of convergence than $\| \| \nabla(v - u) \| \| ^2$. In practice, we can minimize the majorant with respect to y^* only once on a sufficiently big subspace of $H(\text{div}; \Omega)$ to find some good approximation \bar{y}^* of p^* and then reuse this \bar{y}^* and obtain guaranteed and very tight bounds on the error in energy and combined energy norm. To illustrate these ideas, for the first example we recomputed the value of the majorant $M_{\oplus}^2(v, y^*)$ on all mesh levels (sequence of meshes is the same one from Tables 1, 2, 3) using the flux \bar{y}^* that we obtained through the patchwise reconstruction with equilibration at the last level, 11,

where the mesh consists of 386 185 elements. This \bar{y}^* gives a very good approximation to the exact flux p^* and thus the error in $\text{div } \bar{y}^*$ at all adaptation levels before level 11 is much smaller relative to the error measured in energy or combined energy norm. As a consequence, the ratio $D_F(v, -\Lambda^* \bar{y}^*)/M_{\oplus}^2(v, \bar{y}^*)$ is small and increases from around 4% to its final value of 73% at level 11. The respective efficiency indexes with respect to the energy and combined energy norms are given in Table 9. This time, the majorant $M_{\oplus}^2(v, \bar{y}^*)$ gives a much tighter bound on the error in energy and combined energy norm and the efficiency indexes increase from around 1 to their final values at level 11 of 3.3889 and 1.9206, respectively.

Table 9: Example 1 (2D)

Example 1 (2D): $k_1 = 0.15, k_2 = 0.4, \epsilon_1 = 1, \epsilon_2 = 100$						
# elements	$\frac{D_F(v, -\Lambda^* y^*)}{M_{\oplus}^2(v, y^*)} [\%]$	$I_{\text{Eff}}^{\text{CEN,Low}}$	$I_{\text{Eff}}^{\text{CEN,Up}}$	$I_{\text{Eff}}^{\text{E,Up}}$	$P_{\text{rel}}^{\text{CEN}} [\%]$	True rel. error in CEN [%]
196	15.8135	0.70520	1.08700	1.08740	38.5074	36.4137
347	3.61970	0.70640	1.01760	1.01870	22.1410	21.8386
630	3.24520	0.70650	1.01570	1.01800	15.5098	15.4285
1315	2.99700	0.70980	1.01930	1.02350	11.3338	11.2565
2865	5.11630	0.71080	1.03190	1.03970	8.41663	8.36086
5938	9.91240	0.71310	1.06250	1.08000	5.75210	5.69982
12006	19.9535	0.70580	1.11560	1.15160	4.11607	4.12246
24571	35.1659	0.69030	1.21230	1.29130	2.89890	2.96931
48483	45.0879	0.70940	1.35380	1.52340	2.23724	2.23000
97423	59.5529	0.69360	1.54240	1.91030	1.69993	1.73298
192905	68.6293	0.69130	1.74560	2.51110	1.39059	1.42237
386185	73.0132	0.70550	1.92060	3.38890	1.23821	1.24105

5 Conclusions

We proved the existence and uniqueness of a solution u of the nonlinear elliptic Problem (1.1), which appears in context of solving the nonlinear PBE numerically by two- or three-term regularization. We further proved an $L^\infty(\Omega)$ a priori bound on the (regular component of the) solution u (of the PBE), established an analogue of Cea's lemma, cf. (3.34), and used it to prove unqualified convergence of the P_1 Lagrange FEM under uniform mesh refinement.

As a main result we derived the identity (3.27) by finding the explicit form of the terms in the abstract relations (2.7) and (2.11). It defines a natural error measure for the considered class of problems and is the basis for fully computable guaranteed tight bounds on the global errors (see Table 8).

A big advantage of our approach is that it can be used for any conformal approximation ($P_1, P_2, \text{IGA}, \dots$) and that there are no local or global constants present in the estimates for the error in energy and combined energy norm (CEN). Demonstrated by our theoretical findings as well as by the presented numerical tests, good efficiency indexes/tight bounds on the errors, require a flux reconstruction with equilibration. The key factor that determines the efficiency index is the ratio $\frac{D_F(v, -\Lambda^* y^*)}{M_{\oplus}^2(v, y^*)}$.

Assuming that

$$D_F(v, -\Lambda^* y^*) \approx D_F(v, -\Lambda^* p^*) + D_F(u, -\Lambda^* y^*),$$

which means that the last term in (3.32) is close to zero, we obtain from (3.27) the estimate

$$I_{\text{Eff}}^{\text{CEN,Up}} \approx \frac{1}{\sqrt{1 - \frac{D_F(v, -\Lambda^* y^*)}{M_{\oplus}^2(v, y^*)}}}.$$

From what we observed, the efficiency index $I_{\text{Eff}}^{\text{E,Up}}$ with respect to the energy norm usually is no more than twice bigger than $I_{\text{Eff}}^{\text{CEN,Up}}$ (assuming we have a good approximation y^* to p^*). Therefore, if during the computations we detect that this ratio is increasing we can apply the so-called estimation with one step delay, i.e compute the value of the majorant $M_{\oplus}^2(v, y^*)$ for the current mesh level with the reconstructed y^* from the next level. Another strategy is to find somehow a good approximation \bar{y}^* of p^* and reuse it on several AMR levels (for example by means of solving the dual problem P^* -maximizing I^* on possibly another mesh). We also conclude that gradient averaging is not appropriate for obtaining good efficiency indexes and that it tends to overrefine the mesh around the interface.

References

- [1] A collection of molecular surface meshes. https://www.rocq.inria.fr/gamma/gamma/download/affichage.php?dir=MOLECULE&name=water_mol&last_page=6. Accessed: 2017-08-18.
- [2] B. Kawohl, M. Lucia. Best constants in some exponential Sobolev inequalities. *Indiana University Mathematics Journal*, 57(4):1907–1928, 2008.
- [3] M. Page D. Praetorius C. Carstensen, M. Feischl. Axioms of adaptivity. *Comput. Math. Appl.*, 67(6):1195–1253, 2014.
- [4] Hank Childs, Eric Brugger, Brad Whitlock, Jeremy Meredith, Sean Ahern, David Pugmire, Kathleen Biagas, Mark Miller, Cyrus Harrison, Gunther H. Weber, Hari Krishnan, Thomas Fogal, Allen Sanderson, Christoph Garth, E. Wes Bethel, David Camp, Oliver Rübel, Marc Durant, Jean M. Favre, and Paul Navrátil. VisIt: An End-User Tool For Visualizing and Analyzing Very Large Data. In *High Performance Visualization—Enabling Extreme-Scale Scientific Insight*, pages 357–372. Oct 2012.
- [5] D. Braess, J. Schöberl. Equilibrated residual error estimator for Maxwell’s equations. *RICAM report*, 2006.
- [6] D. Kinderlehrer, G. Stampacchia. *An Introduction to Variational Inequalities and Their Applications*. SIAM, 2000.
- [7] Cecile Dobrzynski. MMG3D: User Guide. Technical Report RT-0422, INRIA, March 2012.
- [8] F. Fogolari, A. Brigo, H. Molinari. The Poisson-Boltzmann equation for biomolecular electrostatics: a tool for structural biology. *J. Mol. Recognit.*, 15:377–392, 2002.
- [9] F. Fogolari, P. Zuccato, G. Esposito, P. Viglino. Biomolecular electrostatics with the linearized Poisson-Boltzmann equation. *Biophysical Journal*, 76:1–16, 1999.
- [10] G. Stampacchia. Le problème de Dirichlet pour les équations elliptiques du second ordre à coefficients discontinus. *Annales de l’institut Fourier*, 15(1):189–257, 1965.

- [11] H. Brézis. *Functional Analysis, Sobolev Spaces and Partial Differential Equations*. Springer, 2011.
- [12] H. Brézis, F. Browder. Sur une propriété des espaces de Sobolev. *C. R. Acad. Sc. Paris*, 287:113–115, 1978.
- [13] H. Oberoi, N. M. Allewell. Multigrid solution of the nonlinear Poisson-Boltzmann equation and calculation of titration curves. *Biophysical Journal*, 65:48–55, 1993.
- [14] F. Hecht. New development in FreeFem++. *J. Numer. Math.*, 20(3-4):251–265, 2012.
- [15] I. Ekeland, R. Temam. *Convex Analysis and Variational Problems*. North-Holland Publishing Company, 1976.
- [16] I. Sakalli, J. Schöberl, E. W. Knapp. mFES: A Robust Molecular Finite Element Solver for Electrostatic Energy Computations. *J. Chem. Theory Comput.*, 10:5095–5112, 2014.
- [17] K. A. Sharp, B. Honig. Calculating total electrostatic energies with the nonlinear Poisson-Boltzmann equation. *J. Phys. Chem*, 94:7684–7692, 1990.
- [18] Long Chen, Michael J. Holst, Jinchao Xu. Adaptive finite element modeling techniques for the Poisson-Boltzmann equation. *Siam J. Numer. Anal.*, 45(6):2298–2320, 2007.
- [19] K. G. van der Zee M. Feischl, D. Praetorius. An abstract analysis of optimal goal-oriented adaptivity. *SIAM J. Numer. Anal.*, 54(3):1423–1448, 2016.
- [20] M. Holst, J.A. McCammon, Z. Yu, Y. C. Zhou, Y. Zhu. Adaptive finite element modeling techniques for the Poisson-Boltzmann equation. *Commun. Comput. Phys.*, 11:179–214, 2012.
- [21] P. Neittaanmaki, S. Repin. *Reliable Methods for Computer Simulation: Error Control and Posteriori Estimates*. Elsevier, 2004.
- [22] R. E. Showalter. *Hilbert Space Methods for Partial Differential Equations*. Courier Corporation, 2010.
- [23] S. Repin. On measures of errors for nonlinear variational problems. *Russian J. Numer. Anal. Math. Modelling*, 27(6):577–584, 2012.
- [24] S. Kesavan. *Topics in Functional Analysis and Applications*. New Age International (P) Limited, 1989.
- [25] S. Repin. A posteriori error estimation for variational problems with uniformly convex functionals. *Math. Comp*, 69:481–500, 2000.
- [26] J. Valdman S. Repin. Error identities for variational problems with obstacles. *Z. Angew. Math. Mech.*, pages 1–24, 2017.
- [27] H. Si. TetGen, a Delaunay-based quality tetrahedral mesh generator. *ACM Transactions on Mathematical Software (TOMS)*, 41(11), 2015.